



HAL
open science

Deciphering the origins of Bajocian coral ridges in the Paris Basin: Integrated 3D-seismic reflection, near surface geophysics, and sedimentology

Benjamin Brigaud, Benoît Vincent, Marc Pessel, Albane Saintenoy, Hermann Zeyen, Christophe Durllet, Jessica Saïag, Michel Hayet

► To cite this version:

Benjamin Brigaud, Benoît Vincent, Marc Pessel, Albane Saintenoy, Hermann Zeyen, et al.. Deciphering the origins of Bajocian coral ridges in the Paris Basin: Integrated 3D-seismic reflection, near surface geophysics, and sedimentology. 2024. hal-04635083

HAL Id: hal-04635083

<https://hal.science/hal-04635083v1>

Preprint submitted on 4 Jul 2024

HAL is a multi-disciplinary open access archive for the deposit and dissemination of scientific research documents, whether they are published or not. The documents may come from teaching and research institutions in France or abroad, or from public or private research centers.

L'archive ouverte pluridisciplinaire **HAL**, est destinée au dépôt et à la diffusion de documents scientifiques de niveau recherche, publiés ou non, émanant des établissements d'enseignement et de recherche français ou étrangers, des laboratoires publics ou privés.



Distributed under a Creative Commons Attribution 4.0 International License

Deciphering the origins of Bajocian coral ridges in the Paris Basin: Integrated 3D-seismic reflection, near surface geophysics, and sedimentology

Benjamin Brigaud^{1,2}, Benoît Vincent³, Marc Pessel¹, Albane Saintenoy¹, Hermann Zeyen¹, Christophe Durllet⁴, Jessica Saïag¹ & Michel Hayet⁵

¹Université Paris-Saclay, CNRS, GEOPS, Orsay, France

²Institut universitaire de France (IUF), Paris, France

³Cambridge Carbonate Ltd., 1 rue de Varoux, 21120 Marey-sur-Tille, France

⁴Biogéosciences, CNRS, Université de Bourgogne, 21000 Dijon, France

⁵Andra, Route Départementale 960, 55290 Bure, France

*corresponding author, E-mail address: benjamin.brigaud@universite-paris-saclay.fr,
Université Paris Saclay, CNRS, GEOPS, Rue du Belvédère, 91405 Orsay, France

A CC-BY public copyright license has been applied by the authors to the present document and will be applied to all subsequent versions up to the Author Accepted Manuscript arising from this submission.



Abstract

Enigmatic N120° ridges have been identified from 3D seismic reflection imaging of the Bajocian limestones of the eastern Paris Basin. These features may impact flows within the active Middle Jurassic aquifer beneath the Callovian–Oxfordian claystones and marls that host the Underground Research Laboratory (URL) where the Andra (French National Agency for Radioactive Waste Management) is studying the feasibility of a deep repository for radioactive waste.

It is consequently of paramount importance to understand the nature and origin of these ridges, and an integrated study combining (i) classical field sedimentology and stratigraphy, (ii) near-surface geophysics including Ground Penetrating Radar (GPR), electrical resistivity tomography (ERT) and frequency-domain electromagnetics (FDEM), and (iii) seismic refraction has been developed to investigate them.

Facies analysis and a regional sequence stratigraphy interpretation, integrating near-surface geophysical imaging, performed on time-equivalent outcrop sections demonstrate that elongated mounds of coral bioconstructions with hermatypic scleractinian corals developed during the early Bajocian (*Humphriasianum* chronozone) in shallow, warm oligotrophic seawater. These buildups nucleated as patches on giant subaqueous dunes of peloidal and bioclastic grainstones, dipping mostly N30° with N120°-oriented crests. Some of the bioconstructions form buildups up to 15 m high and several hundred meters wide. They are elongated in the main N120° direction of the underlying dunes, although the dispersion of measurements illustrates the complexity of the interfingering structures observed in 3D seismic images. The bioconstructions are progressively overlapped and draped by oncolite-rich alternating marl-limestones that may result from a shift from oligotrophic to mesotrophic conditions probably brought about by a rise in relative sea level. Near-surface geophysics provide insightful supporting evidence to supplement the field work, particularly by imaging the roots of several bioherms, their internal structures, and the infill of the inter-bioherm troughs.

This work demonstrates the critical importance of outcrop analogue studies for resolving subsurface problems and also shows how near-surface geophysical methods can usefully

supplement direct classical field geology investigations. This new characterization of previously enigmatic structures may also help to provide new constraints for the static and dynamic modelling of the Bajocian aquifer.

Keywords: Carbonate, Bajocian, Facies, Bioherm, Coral, Geophysics

PREPRINT

1. Introduction

Small-scale (infra-kilometer) coral-dominated bioconstructions or buildups are very common features in the sedimentary record through several periods of the Phanerozoic worldwide (e.g. Fournier et al., 2005; Kiessling et al., 2002; Koša, 2015; Mancini et al., 2004; Olivier et al., 2008). These features produce marked heterogeneities in carbonate platforms and within reservoirs together with anisotropic fluid flows (e.g. Howarth and Alves, 2016). It is therefore essential to better constrain the origin and development of such bioconstructions in order to improve the characterization of subsurface carbonate prospects (oil and gas exploration and production, geothermal prospects, CO₂ capture and storage, nuclear waste repository, etc.), (Vennin et al., 2003; Wolpert et al., 2022).

At this scale, the emplacement and development of hermatypic scleractinian corals depends on several key factors including eustatism, salinity, temperature, clastic fluxes, turbidity, and nutrient supply (Pomar, 2001, 1991). Their emplacement is also highly dependent on the inherited topography of the substratum (Bourillot et al., 2009; Goldstein et al., 2013; Vennin et al., 2004), which may be driven by: (1) synsedimentary folds or faults (Durllet et al., 2001, 1997; Fournier et al., 2005), (2) halokinetic movements (Martín-Martín et al., 2017; Poprawski et al., 2016; Teixell et al., 2017), (3) karstic reliefs (Schlager and Purkis, 2015), and (4) former sedimentary structures of diverse origins (Droxler and Jorry, 2013; Macintyre, 1972; Nichol et al., 2012; Riera et al., 2023). The latter aspect is probably particularly prevalent on ramp morphologies where seafloor topography contacts are usually limited (Riera et al., 2023). However, this influence of topographic relief derived from sedimentary structures on the development of bioconstructions, although well appraised in modern or recent examples (Droxler and Jorry, 2013), is still poorly documented in the ancient depositional record (>1 Ma) using geophysical data.

In the eastern Paris Basin, the Andra (French National Agency for Radioactive Waste Management) is operating an Underground Research Laboratory (URL) to study the feasibility of subsurface storage of radioactive waste (Landrein et al., 2013; Pagel, 2014). It has conducted a wide spectrum of geological investigations for more than 20 years, including 2D and 3D seismic reflection surveys, well drilling with coring, and the acquisition of complete

high-resolution sets of well logs. The multidisciplinary geological explorations have focused at depth on a 150 m-thick marl formation of Callovian–Oxfordian age (Pagel, 2014), where the URL is located, and to a lesser extent on the surrounding limestone formations (Brigaud et al., 2014b; Carpentier et al., 2014; Vincent et al., 2007). These bounding formations, respectively of Bajocian–Bathonian and Oxfordian–Kimmeridgian ages and ranging from 250m to 300m thick (Landrein et al., 2013), represent two active aquifers whose characterization is obviously critical for safety reasons. Within the Bajocian limestone, 3D seismic reflection surveys conducted in the vicinity of the URL have revealed some peculiar ridges several kilometers long and less than 1 km wide, trending mainly N120° (Bergerat et al., 2007). A deviated well targeted one of these elongated mounded structures and revealed coral-bearing facies (Brigaud et al., 2010, 2009). The N120° direction is not a frequent structural direction in the Jurassic limestones of the Paris Basin (Andre et al., 2010; Bergerat, 1987, 1987; Blaise et al., 2022), and as a consequence, the origin of these ridges remains enigmatic. This direction is notably different from the N10–N20° and N70–N80° synsedimentary faults that influenced the nucleation of early Bajocian coral reefs in the SE Paris Basin and in Burgundy (Durlet et al., 2001, 1997).

This paper sets out the results of a close integration between deep subsurface geology and geophysics (seismic reflection, core data, and logs), near-surface geophysics including Ground Penetrating Radar (GPR), electrical resistivity sections and seismic refraction sections, together with high-resolution sedimentological field work on outcropping Bajocian limestone in quarries of the eastern edge of the Paris Basin. Our first objective is to characterize the N120° ridges as precisely as possible in order to provide insights and constraints for further static and dynamic modelling of the Middle Jurassic aquifer. A second objective is to define the dynamics of the emplacement and development of Bajocian bioconstructions within a detailed paleo-environmental context, in order to determine the main factors controlling the origin of these structures.

2. Geological setting

During the Jurassic, the Paris Basin was an epicontinental sea open to the Tethys ocean to the East and bordered to the West by the possibly exposed landmasses of the Armorican massif and located at tropical to subtropical latitudes (25–35°N; Figure 1A-B). A wide SE–NW intra-cratonic carbonate platform developed over a vast area of Western Europe, extending for more than 2000 km from Spain in the SW to Poland in the NE. In France, this platform encompassed the Aquitaine Basin in SW, the Jura mountains in the East, and Normandy in the West (Figure 1B, Brigaud et al., 2014a).

Bajocian limestones crop out on the eastern side of the Paris Basin, along a NE–SW zone some 5 km wide (Figure 1C). These limestones dip gently (1–2°) toward the center of the Paris Basin and consequently occur at a burial depth of around 700 m below the URL (Figure 1D). A set of 12 outcrops, including quarries and natural outcrops, were selected and studied for the Bajocian series (Figure 1C).

Below the Bajocian limestone and prior to the development of the Jurassic carbonate platform, the *Marnes à Voltzi* Member of Late Toarcian age is made up of siltstone and claystone with thin micaceous sandstone beds. It is overlain by the still Late Toarcian *Grès supraliasiques* Member (Figure 2) which displays a vertical succession of (1) silty claystone, (2) alternating centimeter-thick beds of siltstone and sandstone, and (3) sandstone with sigmoidal cross-bedding (Guillocheau et al., 2002). The *Grès supraliasiques* facies corresponds to deposition in a tide-dominated distal deltaic system with migrating tidal sand dunes. The overlying *Formation ferrifère* or “Minette de Lorraine” (Guillocheau et al., 2002) displays similar facies to the *Grès supraliasiques*, together with iron ooids with a few calcite bioclasts and a carbonate matrix, appearing as lenses within the dominant clastic facies, submitted to tidal dynamics (Teyssen, 1984). Attributed to the Late Toarcian to Aalenian, this formation is present to the North of the study area (in Lorraine, Audun-le-Roman well; Figure 2) and in the South (around Nogent for instance, Figure 1C, Maubeuge, 1956), but is not documented in the center of the study area (Andra well EST-433; Figure 2A). The overlying *Marnes micacées* Member, dated through the Concavum to *Discites* ammonite chronozones of the Aalenian to Bajocian transition (Guillocheau et al., 2002; Thiry-Bastien, 2002), is probably indicative of the

incipient return of a carbonate factory prior to the development of the Jurassic platform. These deposits thicken significantly from the study area, where they are less than 10 m-thick, northwards in Lorraine where they reach about 30 m thick (Figure 2B). The *Calcaires d'Ottange* Member is composed of bioclastic grainstones with undulated bed planes (Lathuilière, 2005), which are the earliest evidence of the establishment of the Middle Jurassic carbonate platform in the eastern Paris Basin. This member occurs in Lorraine and passes laterally to the South, in the study area, into sandy limestones interbedded with thin marls locally named *Calcaires sableux de Haye* and dated from the *Laeviuscula* ammonite chronozone of the early Bajocian (Lathuilière et al., 2003), which are, however, not always recorded. The *Calcaires à Entroques* Formation comprises cross-bedded, crinoid-rich bioclastic limestones (Guillocheau et al., 2002; Lathuilière, 2005; Lathuilière et al., 2003), dated through the *Propinquans* to *Humphriesianum* chronozones of the early Bajocian (Durlet and Thierry, 2001; Lathuilière et al., 2003). Although relatively thin in the study area, and locally absent, the crinoid-rich packstones to grainstones of this formation are strongly anisopachous, sometimes reaching up to 30 m thick in Lorraine (*Calcaire de Haut-Pont*, Figure 2B) or in the Burgundy High where crinoid fragments accumulate in large sandwaves or in wide prograding slopes sheltered behind pre-existing reliefs (Durlet, 1996; Durlet et al., 2001, 1997; Durlet and Thierry, 2000). The *Oolithes à Clypeus angustoporus* is a member consisting of a relatively thin array of peloidal and bioclastic limestone, subsidiary oolitic, that is sometimes difficult to differentiate from the *Calcaires à Entroques* Formation, and also laterally equivalent northwards to the *Calcaire de Haut-Pont*.

The *Calcaires à Polypiers* Formation, dated from the *Humphriesianum* chronozone of the early Bajocian (Durlet, 1996; Lathuilière, 2000a; Mangold et al., 1994) is subdivided into three members in the study area (Geister and Lathuilière, 1991; Guillocheau et al., 2002; Thiry-Bastien, 2002):

The *Calcaires à Polypiers inférieurs* Member contains bioherms from several meters to a maximum of 15 m-thick, with an overall low diversity of corals (Geister and Lathuilière, 1991; Lathuilière, 2000b, 2000a; Lathuilière and Marchal, 2009);

The *Oncolithe cannabine* Member, which corresponds to two separate members in Lorraine to the North (Figure 2B), is dominated by argillaceous limestones with thin marly interbeds, containing oncoids encrusted by nubecularid foraminifers, along with bivalves and rarer belemnites and ammonites.

The *Calcaires à Polypiers supérieurs* Member consists of cross-bedded bioclastic grainstones with bivalves and crinoids, exhibiting small (less than 1 m) bioherms and biostromes.

The *Marnes de Longwy* Formation is characterized by alternating marls and decimeter-thick beds of argillaceous limestones, and varies widely in thickness from a few meters around Neufchâteau to more than 30 m in the EST-433 well (Figure 1C). It is very rich in brachiopods and also contains some nubecularian oncoids, bivalves, and ammonites indicative of the late Bajocian *Niortense* chronozone (Mangold et al., 1994).

Structurally, the study area is located North of the main E-W Vittel fault, bounding the southern Morvan-Vosgian and Northern Saxon-Thuringian Hercynian terranes, which form the substratum of the Mesozoic series in the eastern Paris Basin. This fault line acted as a normal fault in the Hercynian substratum, and also as a strike-slip fault during the Permian, marking the southern boundary of the Sarre-Lorraine coal basin (Elion et al., 2005). It was probably reactivated during the Jurassic, especially during the Toarcian and Aalenian (Collin and Courville, 2006; de Graciansky and Jacquin, 2003; Durllet et al., 1997; Jacquin et al., 1998; Jacquin and de Graciansky, 1998; Thiry-Bastien, 2002; Vincent, 2001). The Metz fault, located to the North of the study area, is another NE-SW Hercynian feature separating two terranes, the Saxon-Thuringian block to the South, and the Rheno-Hercynian block to the North. It probably impacted sedimentation during the Jurassic, including the Oxfordian (Carpentier et al., 2007). Closer to the URL, within the study area, the main structural feature is the Gondrecourt-le-Château graben (Figure 1C). It is a 30 km-long NNE-SSW structure up to 1500 m thick indicating an atypical sedimentary succession and with vertical displacements of up to several tens of meters (Pagel et al., 2018). Recent U-Pb dating of calcite breccia and veins of the SE Gondrecourt-le-Château graben indicates a two-stage development of the trough, first during the Lutetian and then during the Rupelian (Pagel et al., 2018). The Joinville graben is a very similar structure to the Gondrecourt-le-Château graben, trending in the same

direction and of similar, although slightly shorter, dimensions and reflecting the same dynamic evolution (Figure 1C). U-Pb analyses of tension gashes in the Jurassic limestones, including the *Calcaires à Polypiers* Formation, yield the same ages from Lutetian to Rupelian (Blaise et al., 2022). A first cluster of ages records the far-field onset of the Pyrenean compressional phase during the Lutetian–Bartonian. A second cluster of ages around 33 Ma is related to extensional deformation and the opening of the European Cenozoic Rift System (Blaise et al., 2022). A number of NNW–SSE faults also form a kind of relay between the above-mentioned grabens (Elion et al., 2005). Close to the study area, the N170° Marne faults (Figure 1C) extend over about 100 km and show a cumulated vertical displacement of about 100 m within the Mesozoic sediments.

3. Methods

3.1. 3D seismic reflection

The 3D seismic reflection data that first revealed the Bajocian ridges below the URL were acquired in two phases. A first phase in 1999 was performed by CGG over 4.35 km², in the immediate vicinity of the URL (Figure 1D). The source was a vibroseis source generating a signal in the 19–120 Hz bandwidth. Recording time was 1.5 s with a sampling step of 1 ms, the inter-trace distance was 25 m, and the bin size was 12.5 x 12.5 m. The ridges appeared at the bottom of the Middle Jurassic limestone as N120° elongated antiforms about 10 m in height, and with an approximate wavelength of 300 m (Bergerat et al., 2007; Cuilhé and Bruneton, 2003; Dépré et al., 2003; Drouiller and Guillemot, 2005; Elion et al., 2005).

A second, larger 3D cube of 37 km² was acquired in 2010 by CGG, slightly to the North, targeting a zone for a more in depth investigation to define the location of the potential repository site. The active spread was composed of 12 receiver lines with 120 stations on each line. The receiver and source lines were perpendicular, and their relative spacing was respectively of 80 m and 120 m. The receiver and source point spacing was 20 m. The source was a vibroseis source generating a sweep signal in the 12–140 Hz frequency range,

logarithmically ascending with a slope of 6 dB per octave and upper and lower cosine tapers of 500 ms long. The bin size was 10 x 10 m.

There is no overlap between the two blocks which are, however, linked by a 2D seismic line (10EST01; Figure 1D). A spectral analysis of the seismic data was conducted to check the consistency of the data content between the two cubes. The dominant frequency varies between 75 and 93 Hz, which corresponds to a vertical resolution of 13 to 16 m (assuming that the vertical resolution is approximately $\lambda/4$, with $\lambda=v/f$), for an average carbonate velocity within the Middle Jurassic limestone of 5100 m/s (Brigaud et al., 2010).

3.2. Well data

The EST-433 well is a deep vertical well drilled about 2 km to the NW of the main 3D seismic block (Figure 1D). It is a sedimentological reference that has been extensively studied and described (Landrein et al., 2013), in particular for the Middle Jurassic carbonates (Brigaud et al., 2014b, 2009).

Deviated by about 60° within the Bajocian limestone, another well (EST-210) was designed and drilled to target the ridges (Figure 1D; Rebours et al., 2004). A vertical seismic profile (VSP) was acquired along the well by SCHLUMBERGER in 2004. This VSP was acquired with sources at the surface (vibrating Merte M22 apparatus) and three receivers within the well, spaced 15 m apart, which were shifted along the well trajectory by 5 m for each shot. The recording time was 1900 ms with a sampling step of 2 ms, for a total of 354 shots and 1105 used traces. Brigaud et al. (2014a, 2014b, 2010) published the sedimentological descriptions and a full set of petrophysical analysis for the Middle Jurassic limestone penetrated by this well.

The main seismic horizons were tied to well EST-433 (Figure 2A; Landrein et al., 2013; Mari and Yven, 2014). Several attributes were used in order to image the N120° ridges as clearly as possible, such as azimuth, dip, dip azimuth, and discontinuity. Isochron and isopach maps were constructed and used together with attribute maps.

3.3. Near-surface geophysics

Four near-surface geophysical techniques were used in selected quarries (Attignéville, Beaufremont, Rouvres-la-Chétive, Sommerécourt; Figure 1C) in order to characterize as far as possible the ridges under investigation. The techniques were (1) Ground Penetrating Radar (GPR), (2) Electrical Resistivity Tomography (ERT), (3) Frequency Domain Electromagnetics (FDEM), and (4) seismic refraction. All the instruments used belong to the GEOPS laboratory at Paris-Saclay University.

GPR is increasingly used in carbonate successions (Dagallier et al., 2000; Jorry and Bièvre, 2011) for investigating the physico-chemical properties of rocks at depths between 0 and 5 m. It records the travel time in nanoseconds (ns) between emitters and receivers of electromagnetic pulses. A total of 19 sections were acquired with a RAMAC Mala using shielded antennas centered at 250 MHz.

ERT sections were acquired with an IRIS Instruments multi-electrode system (Syscal Pro), using 48 electrodes at 1 m spacing. The Wenner protocol was used in order to optimize both acquisition for an investigation depth of about 10 m and the signal/background noise ratio. Five sections were acquired for which the apparent resistivity data were inverted with ResIPy (Blanchy et al., 2020).

Five FDEM profiles were produced with a Slimgram multi-frequency system (110 Hz–56 kHz; PROMIS, IRIS instruments), and a distance of 20 m between receiver and transmitter. Measurements of high frequencies (>14 kHz) included substantial background noise rendering them useless. FDEM soundings were inverted separately and integrated to obtain a pseudo-2D section with the IX1D Interpex© software.

Five seismic sections were acquired using DMT-Summit 36 traces equipment. Seismic waves were generated on each line using a 4 kg hammer striking a steel plate. Shot point spacing was 4 m and propagation of P waves was recorded with 60 Hz geophones laid out every 2 m with a sampling frequency of 8 kHz. The data were treated and inverted using PyReFra software (Zeyen and Léger, 2024).

3.4. Sedimentology and sequence stratigraphy

Facies were classically described in the field where outcrop sections were built identifying lithology, textures, allochems, and sedimentary structures. These macroscopic descriptions were supplemented by microscopic investigations of 51 carbonate stained and blue epoxy-impregnated thin sections. Depositional environments were interpreted through the integration of macro and microfacies information on textures, skeletal and non-skeletal grains, sedimentary structures, and ichnotraces.

The vertical transformations in depositional environments along the sections analyzed illustrate changes in the accommodation/sedimentation (A/S) ratio (Homewood et al., 1999). Terminology and interpretation of the sequence stratigraphy follow general principles (Catuneanu et al., 2011), applying the concept of transgressive-regressive sequences (T-R; Embry and Johannessen, 1992). Cycles or sequences of A/S ratio variations are bounded by maximum regressive surfaces (MRS), which may correspond to sequence boundaries (SB). Within the cycles or sequences, maximum flooding surfaces (MFS) separate a transgressive phase or transgressive systems tract (TST; $A/S > 1$, indicated conventionally by a blue triangle) from a regressive phase or regressive systems tract (RST; $A/S < 1$, red triangle).

In addition to sedimentological sections and sequence stratigraphy correlations, high-resolution photographs of the quarries were acquired in order to build photo-panoramas that were interpreted using the established sequence stratigraphic scheme.

4. Results

4.1. Depositional environments: descriptions and interpretations

The sedimentological work made it possible to identify six facies that were grouped into two facies associations interpreted in terms of depositional environments. The entire Lower Bajocian succession could be observed in Attignéville quarry (Figure 3A).

The first facies association FA1 comprises three facies (Figure 3B-F; Table 1): (1) black silty claystone to siltstone (facies F1a), (2) alternating packstone or grainstone with marls and oncoidal/coral fragments (facies F1b), and (3) alternating marls and bioclastic packstone or

grainstone (facies F1c). Facies F1a displays several kinds of sedimentary structures such as thinning-upward thin layers of siltstone or very fine sandstone and current ripples. Bioturbation is also common with *Planolites* ichnotraces in particular. The grainy facies of facies F1b are composed of oncoids with encrusting *nubecularia* foraminifers in their cortex (Figure 3E), but they also contain bivalves, crinoid ossicles, rare brachiopods, rarer ooids and/or peloids, silt-sized quartz grains, and, locally, coral fragments. The grainstone beds within the alternating marls-limestones of facies F1c are composed of bivalves, echinoderms, and silt- to sand-sized quartz grains (Figure 3F). They appear locally as more or less discontinuous lenses with erosional bases, and with internal Hummocky Cross-Stratification (HCS; Figure 3C-D). Facies association FA1 is definitely characteristic of mid to outer ramp environments, influenced by episodic, but common, storm-related hydrodynamics, with the individual facies indicating proximal-distal and lateral variations within this environment. The second facies association FA2 comprises three facies (Figure 3G-H; Table 1) including: (1) coral bioconstructions (facies F2a), (2) bioclastic grainstone to rudstone (facies F2b), and (3) cross-bedded peloidal/oolitic and bioclastic grainstone (facies F2c). The bioconstructions of F2a consist of dome-shaped bioherms reaching 15 m in thickness and a maximum lateral extent of more than 100 m (Figure 3A), where scleractinian corals are the main building organisms (Geister and Lathuilière, 1991; Lathuilière, 2000b, 2000a). Lamellar/tabular (*Isastrea* genus) and platy forms dominate in the bioherms, but domal and even branching forms are present as well (Figure 3G). Lens-shaped biostromes dominated by platy colonies are also observed. The faunal assemblage also contains crinoids, bivalves, bryozoans, and gastropods. Corals are encrusted by micritic microbialites, displaying planar laminae composed of dark micrite with undetermined micro-encrusting organisms (Olivier et al., 2007, 2006) and a few serpulids. The F2b bioclastic grainstone to rudstone contains oncoids, peloids, intraclasts, fragments of corals, echinoderms, bivalves, bryozoans, brachiopods, and rare serpulids and gastropods. Locally, this facies exhibits sigmoidal cross-bedding forming dunes up to several decimeters high. This facies is coarse (rudstone) when close to the bioconstructions, where it results from the dismantling of bioherms, and where it is arranged in prograding bodies fining away from the bioherms. The F2c grainstone contains ooids and

overall abundant peloids, as well as various bioclasts including fragments of echinoderms, corals, bivalves, and bryozoans (Figure 3H). It invariably occurs in large cross beds corresponding to giant subaqueous dunes (Dalrymple and Rhodes, 1995). Facies association FA2 is characteristic of relatively high-energy environments in an inner to mid ramp setting.

4.2. Regional stratigraphic architectures: outcrop correlations

A transect was constructed using nine selected outcrop sections to interpret a stratigraphic scheme (Figure 4). Above the early Jurassic *Marnes micacées* Member, within which is located a 3rd order maximum flooding surface, the echinoderm-rich bioclastic grainstone to rudstone facies (Facies F2b, *Calcaires à entroques*) and cross-bedded oo-bioclastic grainstone (Facies F2c, *Oolithes à Clypeus angustiporus*) constitute the first significant shallow marine carbonate deposits of the Jurassic in the study area (Brigaud et al., 2014a). Within this succession of dominantly shallow marine facies, some interdigitation of open marine echinoderm-rich limestones and marl interbeds (Facies F1c) is also recorded. These are followed, in places, by the development of coral boundstones appearing as meter-scale biostromes or bioherms with dominantly platy corals, as at Marnay or Attignéville (Figure 4), or larger bioherms with a greater diversity of corals, as in the Sommerécourt, Rouvres-la-Chétive, Bourg-St-Marie, and Viterne outcrops (Figure 4). In the Rouvres-la-Chétive quarry, the coral bioherms are emplaced on the top of giant oo-bioclastic cross-bedding (*Oolithes à Clypeus angustiporus* Member), a system described in more detail hereafter. In between the bioconstructions, a continuous record of locally cross-bedded, echinoderm-rich, grain-supported bioclastic facies (facies F2b) is observed such as in the Ozières outcrop (Figure 4). This 12–20 m-thick succession illustrates an overall 3rd order regressive systems tract, which ends with a net maximum regressive surface, characterized in many places by a submarine hardground with no evidence of subaerial exposure (Figure 4).

Above that surface, bioclastic oncolite-rich packstone with marl interbeds (Facies F1b) are deposited across the entire study area, but are anisopachous, ranging from 4 m (e.g. Viterne) to about 10 m (e.g. Rouvres-la-Chétive; Figure 4). These deposits record a 3rd order transgressive systems tract, whose maximum flooding surface is almost impossible to

accurately spot within the succession of oncoid-rich facies. The regressive systems tract of this 3rd order cycle is characterized by another system of echinoderm-rich grainstone (facies F2b) with local cross-bedding. Meter-scale biostromes with platy corals (facies F2a) are interbedded in these grain-supported facies, capped in most of the quarries by another hardground with no evidence of subaerial exposure, and interpreted as the maximum regressive surface (e.g. Jainvilotte; Figure 4). The latter is overlain by the fine-grained limestones and marls (facies F1a) of the *Marnes de Longwy*, recording a pronounced transgression (e.g. Attignéville; Figure 4).

4.3. Near-surface geophysical responses of facies associations and facies: a review from key sites

4.3.1. Attignéville quarry: Facies association FA1

Facies association FA1 has been investigated in Attignéville quarry where the *Marnes micacées* Member crops out at the bottom, displaying 2.5 m of facies F1a claystone to siltstone (Figure 5A-B). These deposits are overlain by the 2m-thick *Calcaires sableux de Haye*, corresponding to bioclastic grainstone (facies F1c). ERT and FDEM profiles were acquired just above the outcrop in the second floor, along the same section (Figure 5).

The ERT section acquired in the quarry shows that the low resistivity values, mainly ranging between 30 and 500 Ohm.m, correspond to facies F1a, whereas slightly higher values from 500 to 1000 Ohm.m correspond to F1c (Figure 5A-C).

An FDEM profile is used to measure resistivities at greater depth (Fig. 5D). From 0 m to 5 m depth, resistivity values range between 50 and 400 Ohm.m and correspond to facies F1a and F1c. Even lower resistivity values of 10 to 70 Ohm.m are measured below, from 5 m to 13 m, and could correspond to facies F1a of the *Marnes micacées* Formation (Figure 5D; Table 1). Below this and down to 20 m, the resistivity of 50–500 Ohm.m could correspond to the *Grès supraliasiques* facies according to regional well data (Guillocheau et al., 2002).

4.3.2. Signature of coral bioherms and surrounding sediments: Facies association FA2

Facies association FA2 was studied in three different quarries.

Beaufremont quarry

Beaufremont quarry displays a bioconstruction (facies F2a) of a minimum thickness of 9 m, and 40–50 m in width (Figure 6A-B). The top of the bioherm is a zone of interdigitation between true coral facies and grain-supported facies F2b of the *Oncolithe cannabine* (Figure 6A-B), illustrating a progressive demise of the bioconstruction. Reworked coral rubble is observed in the onlap zone (F2b; white arrows – Figure 6A). Alternating marl-limestone of the *Oncolithe cannabine* Member (facies F1b) onlaps the coral bioherm and ultimately drapes it continuously.

On the GPR profile 6 acquired at the top of the bioherm, the *Oncolithe cannabine* (facies F2b) is characterized by chaotic reflectors with internal diffraction hyperbolas on the GPR sections, whereas the surrounding and overlying marl-limestone alternations (facies F1b) are imaged as very continuous parallel reflectors (Figure 6C; Table 1). The onlaps observed in the quarry are clearly revealed by the GPR (Figure 6C; – white arrows; Table 1).

ERT section 2, also acquired at the top of the bioherm, shows very high resistivity values of 1000–2000 Ohm.m in the bioconstructed facies (F2a), and lower values of 200–400 Ohm.m in the surrounding F1b facies (Figure 6D; Table 1). The resistivity of the grainy facies F2b, including material dismantled from the bioherm, ranges from 500 to 1200 Ohm.m.

Another bioherm is present in this quarry, but only 2 m of it crop out (Figure 7A-B). Two ERT sections (profiles 3 & 4 Figure 7A-B) were realized on the quarry floor showing that the base of the bioherm is located approximately 5 m below this floor and is characterized by high resistivity values up to and around 1000 Ohm.m (Figure 6C; Figure 7C). The surrounding relatively resistive succession most probably corresponds to the F1b facies (Figure 7C). The uppermost 2–3 m of the sections displays very low resistivity values below 100 Ohm.m, probably corresponding to a bench floor (Figure 7C).

In this site, the FDEM section on the quarry floor does not allow us to distinguish between the bioconstructed facies F2a and the surrounding marl-limestone alternations of facies F1b, both of which display a wide range of overlapping resistivity, from 300 to 1000 Ohm.m (Figure 7D; Table 1). The uppermost part of the FDEM section also exhibits very low values, below

100 Ohm.m, confirming the embankment layer. On the contrary, the GPR section allows us to clearly distinguish the bioherm from the surrounding interbedded marls and limestones (Figure 7E).

A seismic refraction profile was acquired on the floor of this quarry, between the two faces illustrated in the panoramas of Figure 6 and Figure 7 (Figure 8A-B). The uppermost meter of the profile, showing low velocities (<1000 m/s), confirms a thin bench floor. Below, three distinct patches of higher velocities (2000–3000 m/s), definitely illustrate some coral bioherms (Facies F2a; Figure 8A-B). The largest high velocity patch on the SSE of the seismic profile (A in Figure 8B) corresponds to the rooting of the bioherm illustrated in Figure 6, whereas a smaller patch on the NNW side of the profile (C in Figure 8B) likely corresponds to the base of the small bioherm illustrated in Figure 7. The third patch (B in Figure 8B) is not visible on the quarry faces. The base of the three bioherms is confirmed to be 4–5 m below the quarry floor (Figure 8B). A 20 m-wide trough is imaged on the profile between the high velocity patches A and B, and is filled with a lower velocity material (1000–1500 m/s; Figure 8B), probably corresponding to facies F1b of the *Oncolithe cannabine*.

Rouvres-la Chétive quarry

In this quarry, a first face (NE–SW) displays a lenticular-shaped bioherm that developed above a sedimentary body composed of oo-bioclastic facies F2c (*Oolithes à Clypeus angustiporus* Member), displaying large-scale cross-bedding with inclined sets dipping steeply to the NE with a N30° direction (Figure 9A-C). In front of the bioherm, a trough some 10 m-deep with an erosional base is filled with alternating fine limestones and marls of facies F1b, also showing beds of bioclastic sediments containing components derived from the dismantling of the bioherm and downlapping on the basal surface (Figure 9A-D). The bioherm is progressively overlapped by the same alternations of the *Oncolithe cannabine* (Figure 9A-D). On a NW–SE face of the quarry, the same bioherm also appears on top of prograding sets which dip N30° at a lower angle (Figure 9F-G). The sets here show a complex internal organization with cross-bedding and erosional surfaces between and within sets. On this face, the bioherm does not evolve laterally towards other facies, but pinches out downward on the slope of the

topmost set (Figure 9F-G). It is also overlapped and finally draped by the fine planar stratified sediments of the *Oncolithe cannabine*. This succession is overlain by the cross-bedded grain-supported facies of the *Calcaires à Polypiers supérieurs* Member.

Two seismic refraction profiles were acquired in the quarry, behind the SW-NE face illustrated in Figure 9A-B (Figure 10A). Profile S3 oriented SW-NE shows a clear boundary between relatively high velocity facies (2000–3000 m/s) and the overlying lower-velocity facies (<1800 m/s) at around 10 to 12 m depth (Figure 10B). This boundary plunges significantly to the NE between 45 m and 55 m along the profile, which corresponds to the dip of the large cross beds observed on the SW-NE quarry face (Figure 9C). The velocity contrast boundary consequently corresponds to the contact between facies F2c of the cross beds and the overlying facies F1b of the *Oncolithe cannabine*. Profile S4 reveals the same velocity contrast boundary, but gently dipping from N to S from 4 m-deep to about 20 m-deep (Figure 10C). This could be interpreted as the image of the stoss side of a giant dune, the cross beds of which are observed on the quarry faces. Higher velocity patches (2500–3000 m/s) are visible, deforming the velocity boundary and forming positive 3–4 m-high reliefs (A and B in Figure 10C). They could likely be interpreted as coral bioherms (facies F2a) developing on the cross beds, as they are observed on the quarry faces (Figure 9).

Sommerécourt quarry

This quarry reveals a main bioconstruction some 10 m-high with many corals in place, extending over more than 100 m along a SSW-NNE oriented face (Figure 11A). On the flanks of the major bioherm (facies F2a), as well as laterally, smaller meter-scale patches are observed (Figure 11C-D). The bioherms are separated by troughs filled with bioclastic facies F2b (Figure 11C-F). The bioherm is built from platy and branching corals, with subsidiary encrusting micritic microbialites which include microfabric composed of planar micritic laminae (sensu Vennin et al., 2021) and serpulids. A smaller less accessible bioherm is also visible on the NNE extreme part of the face (Figure 11A-D). Another part of the bioherm is observed in the SE part of the quarry, in another cliff (Figure 11A-B). The line between the occurrences of the coral bioherm high along the two cliffs is oriented N120°, giving a possible

direction of the coral ridge (Fig. 11A-B). A second view of the SSW–NNE face allows us to clearly observe the coral ridge on the first cliff while, on the second cliff, triangular fractures appear at the apex of the coral ridge, highlighting its N120° orientation.

A GPR section was acquired on the second floor of the quarry, parallel to the main stratigraphic photopanorama (Figure 11C-D). The GPR image is very similar to the interpreted stratigraphic panorama, with two positive structures corresponding to the observed bioherms (facies F2a), characterized by chaotic reflectors on either side of the section, and showing a set of strong high-amplitude reflectors at their top (Figure 12A-B). They are separated by an inter-bioherm trough with moderate amplitude parallel reflectors, some overlapping the bioherms. The base of the trough seems to show slightly higher amplitude reflectors than the upper part, which respectively correspond to facies F1b and F2b filling the trough, observed in the panorama (Figure 11C-D).

The FDEM section, conducted on the quarry floor and investigating the 20 m depth below, reveals three different zones, here named boxes (Figure 12C). Boxes 1 and 1', from 2 to 8 m deep, display the lowest resistivities between 20 and 80 Ohm.m. Boxes 2 and 2' display intermediate resistivities ranging from 100 to 200 Ohm.m. Finally, boxes 3 and 3' have the highest resistivities reaching up to 1000 Ohm.m, with the highest values being at the base of the boxes. These latter zones could be interpreted as tight oo-bioclastic grain-supported and cross-stratified facies F2c, similar to that observed in Rouvres-la-Chétive quarry. Thus, these two patches could correspond to large cross beds possibly serving as a substratum for the bioherms.

The seismic section (Figure 12D), investigating 20 m depth below the quarry floor, identifies a thin 0 to 2 m-thick uppermost layer with velocities below 1.5 km/s, probably corresponding to either a bench floor and underlain by some 5 m of porous, altered and fractured limestone probably of facies F2b, with velocities between 3 and 3.5 km/s (Figure 12D). Velocities between 4 and 5 km/s most likely correspond either to biohermal facies F2a or to tightly cemented oo-bioclastic facies F2c of the *Oolithes à Clypeus angustiporus* Member. These velocities are found at shallower depths (below 4 to 6 m) near the edges of the transect and

at greater depths (more than 8 to 10 m) in the middle of the section, illustrating an undulation of up to 4 m.

The ERT section reaches a depth of 8 m below the quarry floor (Figure 12E). The first meter displays low resistivity values between 100 and 300 Ohm.m, probably corresponding to a bench floor, as suggested by the seismic profile (Box 1). Two patches of higher resistivity occur below on either side of the section, with values ranging between 600 and 1000 Ohm.m, that could correspond to biohermal facies F2a (Boxes 2 and 2'). Between the high-resistivity patches, a lower resistivity zone is visible, with values ranging between 300 and 400 Ohm.m (Figure 12E, Box 3). This zone could correspond to bioclastic grainstone to rudstone, with interbedded coral debris (F2b).

4.4. Deep geophysics and well data

This section describes some of the findings from the 3D seismic reflection and well data acquired near the URL of Bure. The dip attribute extracted at the top of the Middle Jurassic does not display any specific features (Figure 13A), indicating that the interval is not affected by structural features at this scale of observation. The same attribute extracted at the top of the *Calcaire à Polypiers* Formation reveals a number of elongated kilometer-scale N120° trending structures (Figure 13B). Isochron maps for the same formation also show N120° elongated but more rounded "thicker" structures (Figure 13D). The azimuthal dip attribute map of the top of the *Calcaire à Polypiers* Formation indicates that, for the eastward dipping class, the dip is greater towards the NE (Figure 13C).

The Est-210 deviated well was designed to cut through one of the 3D seismic-imaged N120° lineaments in the laboratory zone (Figures 13 & 14A-B). A full set of logs was acquired along this well, supplemented with a VSP (Figure 14A) revealing an anticline-shaped structure within the *Calcaire à Polypiers* Formation below the well trace (Figure 14C). Below the *Marnes de Longwy* Formation, the cores clearly cut through bioconstructed limestone (Figure 14D), described by Brigaud et al. (2010). In summary, from base to top, between 770 m and 760 m (TVD), boundstones with dominantly platy and subsidiary phaceloid branching corals are

observed (facies F2a). From 760 m to 750 m, cross-bedded peloidal and bioclastic packstones to grainstones with fragments of echinoderms, corals, and bivalves (facies F2b) are present. Above, a 2 m-thick interval of marls with a few limestone beds is recorded; the limestone beds are wackestones to packstones with nubecularian oncoids and fragments of echinoderms, corals, and bivalves (facies F1b). Between 748 m and 739 m, another interval of facies F2b is observed, encompassing a meter-thick zone of small bioherms/biostromes with platy corals.

This cored succession, together with the analogous outcropping levels presented previously, demonstrate that the positive features observed both on the VSP and on seismic reflection lines (Figure 14B), and which correspond to the N120° lineaments of the 3D-seismic image, are elongated coral ridges probably formed by stacked bioherms.

5. Discussion

Through some direct field observation and constrained indirect near-surface geophysical interpretations, it is clear now that the coral bioherms forming the ridges developed on giant subaqueous dunes of the *Oolithes à Clypeus angustiporus* Member, with a N30° progradation and with a crest orientation of N120° (Fig. 15A), guiding the development of the seismic-scale ridges (Figure 13D). Despite this overall constant direction, the structures appear more interfingered than initially thought based on the 1999 URL 3D seismic block alone (Figure 15B-C). The good quality of the 2011 larger seismic block still reveals elongated ridges, but of a more massive aspect (Figure 15B-C), corresponding to positive mounded features located in the lower part of the *Calcaires à Polypiers* Formation (Figure 15A). This is consistent with the outcrops, some 30 km away (Figure 1C), where all the larger-scale bioherms are located in the *Calcaires à Polypiers inférieurs* Member. Importantly, the 2011 seismic block also shows that none of these structures is traceable within the underlying Liasic or Rhaetian series (Figure 16), the basal contact of the *Calcaires à Polypiers* Formation corresponding to a net plane reflector (Figure 16), allowing us to rule out any tectonic rooting. This goes against bioherms aligned above syndimentary faults, as described for example 70 km further South, in the Marne Spring quarries (Durllet et al., 1997). These near-surface techniques on

outcrops are likely to be valuable complements for studies of carbonate bioconstructions in geothermal reservoirs, such as those of the Upper Jurassic in Germany (Wolpert et al., 2022), or carbonate bioconstructions observed on outcrops (Dagallier et al., 2000; Matyszkiewicz et al., 2006).

5.1. Origin of the giant dunes

In Rouvres-la-Chétive quarry, the main dip direction of the sets of giant subaqueous dunes is N30°, although it is not really possible to determine whether these are 2D or 3D dunes (Figure 9), and the main direction of the crest is around N120°. The dune height is estimated between 8 m and 10 m, which gives a possible paleobathymetry of between 47 m and 58 m according to the 17% ratio of Dalrymple and Rhodes (1995).

It is tempting to compare these Bajocian dunes morphologically with some sedimentary features of the Tongue of the Ocean shoal complex in the Bahamas (Rankey and Reeder, 2012). The latter complex consists in a vast number of tidal dunes of variable geometries including giant longitudinal and interfingering systems several kilometers long (Figure 17A-B). In the southern and western parts of this modern analog the average dune length is around 10 km, and their average width several hundreds of meters for bathymetry ranging from 25 m to 75 m (Figure 17B; Rankey and Reeder, 2012). In these places, dunes are separated by deeper troughs of about 1.2 km wide and up to 8 m-deep (Rankey and Reeder, 2012). Such dimensions are similar to the estimated sizes of the giant Bajocian structures visible in the 3D seismic image (Figure 16B-C) and on the outcrops.

Modern and ancient giant dunes are often interpreted as resulting from tidal currents (Anastas et al., 1997; Bastos et al., 2003; Fenster et al., 1990; Malikides et al., 1988; Todd and Shaw, 2009), with frequent modifications of their geometry due to storm events, as in the Bahamas (Rankey et al., 2006 and references therein). In the geological record, these dunes would be mostly recorded in low-stand or early transgressive periods due to the local constriction of tidal currents (Reynaud and Dalrymple, 2012), the slow increase in accommodation space preserving them from systematic erosion. The giant dunes observed

in the Lower Bajocian succession under study were deposited as part of a regressive systems tract and there is no indication of bi-directionality within these structures, showing that a tidal origin is unlikely. Vincent et al. (2021) described and interpreted similar giant dunes in oobioclastic limestones of the Bathonian of the Paris Basin, slightly towards the SE of the study area, and came to the same conclusion. Detailed regional paleogeographic reconstructions (Thiry-Bastien, 2002) show that, during the early Bajocian, the study area overall corresponded to a shallow-water area of a large carbonate platform, with open ocean zones situated to the South (Jura, Bresse graben), to the West (Paris area), and for the closest one to the NE (Souabe basin in Germany). It is likely that such a geographically restricted shallow water zone was subject to strong unidirectional currents bridging the open zones, that may have given rise to the large subaqueous dunes.

5.2. Forcing parameters on the development and evolution of the Bajocian coral bioherms

In the study area, the Aalenian is missing or limited to lenticular deposits which remain undocumented because of poor outcrop conditions. This is probably due to a second order maximum of regression recorded in numerous European basins during the Aalenian (Jacquin et al., 1998). In the eastern Paris Basin and in Burgundy, accommodation was very low during the Aalenian and the earliest Bajocian, preventing significant sedimentation and/or sediment preservation (Durllet and Thierry, 2000). Continuous sedimentation resumed during the *Discites* chronozone, firstly with clay-rich sediments of the *Marnes micacées* Member, probably under oligotrophic to mesotrophic conditions and temperate surface seawater temperatures of 15–20 °C (Figure 18A; Dera et al., 2011). During the *Laeviuscula* and *Propinquans* chronozones, various limestone units (*Calcaires sableux de Haye*, *Calcaires de Hottange*, *Calcaires de Haut-Pont*, *Calcaires à entroques*) usually rich in crinoids, bryozoans, and pelecypods were deposited, indicating slightly warmer waters but still nutrient-loaded and with few distal detrital inputs. During the *Discites* or the early *Humpriesianum* chronozones, more arid and warmer conditions promoted deposition of pure bioclastic and oobioclastic

grainstones (*Oolithes à Clypeus angustiporus* Member), sometimes structured with large cross-beds corresponding to the N120° subaqueous giant dunes (Figure 18B). Later in the early Bajocian *Humpriesianum* chronozone, installation of durable oligotrophic conditions and higher surface temperatures reaching 20–30 °C (Brigaud et al., 2009; Dera et al., 2011) favored the growth of coral bioconstructions (Piuz, 2008).

Bioherms first nucleated on the crests of the giant dunes and then developed to form high relief buildups of up to 15 m (Figure 18C), while the inter-biohermal troughs were filled with bioclastic sediments including material from the dismantling of bioherms (*Calcaires à Polypiers inférieurs* Member). When the available space was reduced, bioherms extended laterally (progradation), which is observed in quarries and partly explains the massive interfingering aspect of the structures. The paleotopographic lows were simultaneously filled with bioclastic sediments (Figure 18D). In the absence of structural roots, in a tectonically quiet period of the intracratonic Paris Basin, the sedimentary-inherited topographies (i.e. subaqueous dunes) played a key role in the emplacement and development of these seismic-scale coral systems.

Another factor favored the progressive bioherm growth on dune crests in the absence of tectonic rooting or syndepositional deformation. In outcrops and cored wells, the top of the *Oolithes à Clypeus angustiporus* facies usually corresponds to a hardground (Figure 4) with pelecypods and worm borings that cross-cut isopachous calcite cements. These marine cements precipitated during the hiatus linked to the discontinuity, as documented further South below many other perforated surfaces in the Lower Bajocian limestones (Durllet et al., 1992; Loreau and Durllet, 1999). These early cements lithified the last decimeters below the top of the dunes. Without such early lithification, the heavy bioherms would have likely progressively deformed the underlying calcarenites and would have sunk into them. As for the chemical and biochemical production of relatively pure oo-bioclastic facies (facies F2b and F2c) constituting the dunes, an arid climate with warm oligotrophic seawater probably promoted the early calcite cementation, among other factors. Submarine hardgrounds are commonly stable substrates for nucleation and growth of coral buildups or reefs, especially

when they cap prominent submarine reliefs where higher photic levels favor photosynthesis (for hermatypic corals) and where currents bring nutrients to the colonies.

The topography was leveled slightly later with oncoïd-rich fine limestone and marl alternations (*Oncolithe cannabine* Member) onlapping and draping the bioherms. This facies probably indicates a return to mesotrophic conditions that were less favorable for scleractinian corals. Later, as evidenced by the regional Jurassic series, it was only from the Late Oxfordian that ecosystems were to allow the development of new big coral bioconstructions (Carpentier et al., 2007).

6. Conclusions

An integrated study associating classical field sedimentology and stratigraphy, near-surface geophysics (including Ground Penetrating Radar (GPR), resistivity (ERT and FDEM)), and seismic refraction has been developed to investigate the Bajocian limestones of the eastern Paris Basin, in order to determine the nature, characteristics, and origin of enigmatic N120° ridges identified at a present-day depth of about 750 m from 3D seismic reflection by the Andra (French National Agency for Radioactive Waste Management).

Classical facies analysis and a regional sequence stratigraphy interpretation have been performed on time-equivalent outcrop sections (quarries), demonstrating that elongated mounds of coral bioconstructions with hermatypic scleractinian corals developed during the early Bajocian (*Humphriasianum* chronozone) in warm oligotrophic and shallow seawater. Some of the bioconstructions form buildups reaching 15 m in height and hundreds of meters in width. They are elongated in the main N120° direction, with, however, a significant spread of measurements illustrating the complexity of the interfingered structures observed in 3D seismic images. The bioconstructions were progressively onlapped and draped by alternating oncoïd-rich marls-limestones that probably resulted from a change from oligotrophic to mesotrophic conditions possibly associated with a relative sea-level rise. Near-surface geophysical data supplement the limited direct observations on quarry faces, with GPR especially providing excellent quality images of the internal bioherm structures and of the infill of the inter-bioherm troughs.

In several outcrops, but especially in Rouvres-la-Chétive quarry, it is observed that coral patches nucleated on large scale cross beds of peloidal and bioclastic grainstones, corresponding to giant subaqueous dunes. Before bioherm development, the tops of these dunes were lithified by isopachous calcite cement, forming submarine hardgrounds and thus stable substrates for buildup growth. The main dip direction of the dune sets is N30°, with a crest direction of around N120°. Near-surface geophysics supplements imaging of the roots of several bioherms that only crop out in part.

This work demonstrates the critical importance of outcrop analog studies for resolving subsurface problems, and it also shows how near-surface geophysical methods can supplement classical field geology investigations. From a more applied perspective, the position and geometry of the dune/bioconstruction complexes also shed new light on the constraints to be applied to static and dynamic modelling of the Bajocian aquifer. These near-surface techniques on outcrops are likely to be valuable complements for studies of coral reefs in geothermal reservoirs.

7. Acknowledgments

This work is a contribution to project No 2011-XV "Origin of N120° structures detected within the 3D subsurface seismic cube: insight from the geophysical and sedimentological study of outcrops of the Middle Jurassic Limestones" of the CNRS *Programme sur l'Aval du Cycle et l'Energie Nucléaire (PACEN)*, and to collaborative project No N87890 "Surface geophysical study of the Bajocian outcrops of the eastern Paris Basin: Contribution to the understanding of structures detected in 3D seismics" between the University Paris-Saclay and the Andra (French National Agency for Radioactive Waste Management). This study has benefited greatly from CNRS and Andra funding. We thank Professor Maurice Pagel for promoting this work on the geology of this area. The authors would like to thank Philippe Courville (Univ. Rennes) for determinations of brachiopod fauna, Thierry Albertin, Christophe Pouzot (BSc students), and Frédéric Hirn (MSc student). They are grateful to Philippe Blanc (Lithologie Bourgogne) for the high-quality thin sections.

8. Data Availability

The data that support the findings in this study are openly available in Recherche Data Gouv repository at <https://doi.org/10.57745/TMB0HR>.

PREPRINT

9. References

- Anastas, A., Dalrymple, R., James, N., Nelson, C., 1997. Cross-stratified calcarenites from New Zealand: subaqueous dunes in a cool-water, Oligo-Miocene seaway. *Sedimentology* 44, 869–891. <https://doi.org/10.1046/j.1365-3091.1997.d01-57.x>
- Andre, G., Hibsich, C., Fourcade, S., Cathelineau, M., Buschaert, S., 2010. Chronology of fracture sealing under a meteoric fluid environment: Microtectonic and isotopic evidence of major Cainozoic events in the eastern Paris Basin (France). *Tectonophysics* 490, 214–228. <https://doi.org/10.1016/j.tecto.2010.05.016>
- Bastos, A.C., Collins, M., Kenyon, N.H., 2003. Morphology and internal structure of sand shoals and sandbanks off the Dorset coast, English Channel. *Sedimentology* 50, 1105–1122. <https://doi.org/10.1046/j.1365-3091.2003.00596.x>
- Bergerat, F., 1987. Tertiary Paleostress Fields in the European Platform in Front of the Alpine Orogen. *Bulletin De La Societe Geologique De France* 3, 611–620.
- Bergerat, F., Elion, P., Frizon de Lamotte, D., Proudhon, B., Combes, P., André, G., Willeveau, Y., Laurent-Charvet, S., Kourdian, R., Lerouge, G., Ott d'estevou, P., 2007. 3D multiscale structural analysis of the eastern Paris basin: the Andra contribution, in: Lebon, P. (Ed.), *A Multi-Disciplinary Approach to the Eastern Jurassic Border of the Paris Basin (Meuse / Haute-Marne)*, Mémoire de La Société Géologique de France. pp. 15–35.
- Blaise, T., Ali Khoudja, S.A., Carpentier, C., Brigaud, B., Missenard, Y., Mangenot, X., Boulvais, P., Landrein, P., Cochard, J., 2022. Far-field brittle deformation record in the eastern Paris Basin (France). *Geol. Mag.* 159, 2095–2109. <https://doi.org/10.1017/S0016756822000772>
- Blanchy, G., Saneiyani, S., Boyd, J., McLachlan, P., Binley, A., 2020. ResIPy, an intuitive open source software for complex geoelectrical inversion/modeling. *Computers & Geosciences* 137, 104423. <https://doi.org/10.1016/j.cageo.2020.104423>
- Bourillot, R., Vennin, E., Kolodka, C., Rouchy, J.-M., Caruso, A., Durllet, C., Chaix, C., Rommevaux, V., 2009. The role of topography and erosion in the development and architecture of shallow-water coral bioherms (Tortonian–Messinian, Cabo de Gata, SE Spain). *Palaeogeography, Palaeoclimatology, Palaeoecology* 281, 92–114. <https://doi.org/10.1016/j.palaeo.2009.07.015>
- Brigaud, B., Durllet, C., Deconinck, J.-F., Vincent, B., Pucéat, E., Thierry, J., Trouiller, A., 2009. Facies and climate/environmental changes recorded on a carbonate ramp: A sedimentological and geochemical approach on Middle Jurassic carbonates (Paris Basin, France). *Sedimentary Geology* 222, 181–206. <https://doi.org/10.1016/j.sedgeo.2009.09.005>
- Brigaud, B., Vincent, B., Carpentier, C., Robin, C., Guillocheau, F., Yven, B., Huret, E., 2014a. Growth and demise of the Jurassic carbonate platform in the intracratonic Paris Basin (France): Interplay of climate change, eustasy and tectonics. *Marine and Petroleum Geology* 53, 3–29. <https://doi.org/10.1016/j.marpetgeo.2013.09.008>
- Brigaud, B., Vincent, B., Durllet, C., Deconinck, J.-F., Blanc, P., Trouiller, A., 2010. Acoustic Properties of Ancient Shallow-Marine Carbonates: Effects of Depositional Environments and Diagenetic Processes (Middle Jurassic,

Paris Basin, France). *Journal of Sedimentary Research* 80, 791–807. <https://doi.org/10.2110/jsr.2010.071>

Brigaud, B., Vincent, B., Durllet, C., Deconinck, J.-F., Jobard, E., Pickard, N., Yven, B., Landrein, P., 2014b. Characterization and origin of permeability–porosity heterogeneity in shallow-marine carbonates: From core scale to 3D reservoir dimension (Middle Jurassic, Paris Basin, France). *Marine and Petroleum Geology* 57, 631–651. <https://doi.org/10.1016/j.marpetgeo.2014.07.004>

Carpentier, C., Brigaud, B., Blaise, T., Vincent, B., Durllet, C., Boulvais, P., Pagel, M., Hibsich, C., Yven, B., Lach, P., Cathelineau, M., Boiron, M.-C., Landrein, P., Buschaert, S., 2014. Impact of basin burial and exhumation on Jurassic carbonates diagenesis on both sides of a thick clay barrier (Paris Basin, NE France). *Marine and Petroleum Geology* 53, 44–70. <https://doi.org/10.1016/j.marpetgeo.2014.01.011>

Carpentier, C., Lathuilière, B., Ferry, S., Sausse, J., 2007. Sequence stratigraphy and tectonosedimentary history of the Upper Jurassic of the Eastern Paris Basin (Lower and Middle Oxfordian, Northeastern France). *Sedimentary Geology* 197, 235–266. <https://doi.org/10.1016/j.sedgeo.2006.10.004>

Catuneanu, O., Galloway, W.E., Kendall, C.G.St.C., Miall, A.D., Posamentier, H.W., Strasser, A., Tucker, M.E., 2011. Sequence Stratigraphy: Methodology and Nomenclature. *Newsletters on Stratigraphy* 44, 173–245. <https://doi.org/10.1127/0078-0421/2011/0011>

Collin, P.-Y., Courville, P., 2006. Sedimentation and palaeogeography of the eastern part of the Paris Basin (France) at the Middle–Upper Jurassic boundary. *Comptes Rendus Geoscience* 338, 824–833. <https://doi.org/10.1016/j.crte.2006.07.011>

Cuilhé, L., Bruneton, A., 2003. Site Meuse/Haute-Marne. Sismique 3D après retraitement 2002. Rapport d'interprétation géologique et structurale (No. C.RP.0BEI.03.002.A). Andra.

Dagallier, G., Laitinen, A.I., Malartre, F., Van Campenhout, I.P.A.M., Veeken, P.C.H., 2000. Ground penetrating radar application in a shallow marine Oxfordian limestone sequence located on the eastern flank of the Paris Basin, NE France. *Sedimentary Geology* 130, 149–165. [https://doi.org/10.1016/S0037-0738\(99\)00105-0](https://doi.org/10.1016/S0037-0738(99)00105-0)

Dalrymple, R.W., Rhodes, R.N., 1995. Chapter 13 Estuarine Dunes and Bars, in: Perillo, G.M.E. (Ed.), *Geomorphology and Sedimentology of Estuaries*, *Developments in Sedimentology* 53. Elsevier, pp. 359–422. [https://doi.org/10.1016/S0070-4571\(05\)80033-0](https://doi.org/10.1016/S0070-4571(05)80033-0)

de Graciansky, C., Jacquin, T., 2003. Evolution des structures et de la paléogéographie au passage Lias-Dogger dans le bassin de Paris d'après les données de la subsurface. *Bulletin De La Societe Geologique De France* 174, 3–17.

Dépré, P., Murillo, J.P., Dupont, R., 2003. Laboratoire souterrain de Meuse/Haute-Marne. Sismique 3D, 2D. Rapport de retraitement (No. D.RP.0CGG.03.001.A). Andra.

Dera, G., Neige, P., Dommergues, J.L., Brayard, A., 2011. Ammonite paleobiogeography during the Pliensbachian-Toarcian crisis (Early Jurassic) reflecting paleoclimate, eustasy, and extinctions. *Global and Planetary Change* 78, 92–105. <https://doi.org/10.1016/j.gloplacha.2011.05.009>

Dercourt, J., Gaetani, M., Vrielynck, B., Barrier, E., Biju Duval, B., Brunet, M.F., Cadet, J.P., Crasquin, S., Sandulescu,

M., 2000. Atlas Peri-Tethys, Palaeogeographical maps, 24 maps and explanatory notes: I-XX. CCGM/CGMW, Paris 1–269.

Drouiller, Y., Guillemot, D., 2005. EST210. PSV Walk-above. Interprétation combinée du PSV avec l'imagerie de paroi FMI et la sismique 3D. Laboratoire de recherche souterrain de Meuse/Haute-Marne (No. D.RP.ADPE.04.1124). Andra.

Droxler, A.W., Jorjy, S.J., 2013. Deglacial Origin of Barrier Reefs Along Low-Latitude Mixed Siliciclastic and Carbonate Continental Shelf Edges. *Annual Review of Marine Science* 5, 165–190. <https://doi.org/10.1146/annurev-marine-121211-172234>

Durlet, C., 1996. Apport de la diagenèse des discontinuités à l'interprétation paléo-environnementale et séquentielle d'une plate-forme carbonatée (PhD thesis). Université de Bourgogne, Dijon.

Durlet, C., Jacquin, T., Floquet, M., 1997. Extensional synsedimentary tectonics during Aalenian and Bajocian on the Burgundy High (France). *Comptes Rendus de l'Académie des Sciences Série IIa: Sciences de la Terre et des Planètes* 324, 1001–1008.

Durlet, C., Lathuilière, B., Aycard, M., 2001. Reef geometries and facies in Bajocian limestones of the Burgundy High (France): Environmental and sequence stratigraphy interpretations. *Eclogae Geologicae Helvetiae* 94, 1–11.

Durlet, C., Loreau, J.P., Pascal, A., 1992. Diagenetic Signature of Unconformities and New Graphic Visualization of Diagenesis. *Comptes Rendus de l'Académie des Sciences Série IIa: Sciences de la Terre et des Planètes* 314, 1507–1514.

Durlet, C., Thierry, J., 2000. Modalités séquentielles de la transgression aaléno-bajocienne sur le sud-est du Bassin parisien. *Bulletin de la Société Géologique de France* 171, 327–339.

Elion, P., Brulhet, J., Leclerc, E., 2005. Le site de Meuse/Haute-Marne: histoire géologique et état actuel (No. C.RP.ADS.04.0022B), Dossier 2005 Référentiel du site Meuse/Haute-Marne Tome 1. Chapitre 8. Andra.

Embry, A.F., Johannessen, E.P., 1992. T-R sequence stratigraphy, facies analysis and reservoir distribution in the uppermost Triassic- Lower Jurassic succession, western Sverdrup basin, Arctic Canada, in: Vorren, T.O., Bergsager, E., Dahl-Stamnes, O.A., Holter, E., Johansen, B., Lie, E., Lund, T.B. (Eds.), *Arctic Geology and Petroleum Potential*, n 2, Special Publication Norwegian Petroleum Society (NPF). pp. 121–146.

Fenster, M.S., Fitzgerald, D.M., Bohlen, W.F., Lewis, R.S., Baldwin, C.T., 1990. Stability of giant sand waves in eastern Long Island Sound, U.S.A. *Marine Geology* 91, 207–225. [https://doi.org/10.1016/0025-3227\(90\)90037-K](https://doi.org/10.1016/0025-3227(90)90037-K)

Fournier, F., Borgomano, J., Montaggioni, L.F., 2005. Development patterns and controlling factors of Tertiary carbonate buildups: Insights from high-resolution 3D seismic and well data in the Malampaya gas field (Offshore Palawan, Philippines). *Sedimentary Geology* 175, 189–215. <https://doi.org/10.1016/j.sedgeo.2005.01.009>

Geister, J., Lathuilière, B., 1991. Jurassic coral reefs of the northeastern Paris Basin (Luxembourg and Lorraine). Presented at the International Symposium on Fossil Cnidaria, p. 112.

Goldstein, R.H., Franseen, E.K., Lipinski, C.J., 2013. Topographic and sea level controls on oolite-microbialite-coralgal reef sequences: The terminal carbonate complex of southeast Spain. *AAPG Bulletin* 97, 1997–2034.

<https://doi.org/10.1306/06191312170>

Guillocheau, F., Robin, C., Mettraux, M., Dagallier, G., Robin, F.-X., Le Solleuz, A., 2002. Le Jurassique de l'Est du Bassin de Paris. *Bull. Inf. Géol. Bass. Paris* 39, 23–47.

Homewood, P., Mauriaud, P., Lafont, F., 1999. Best practices in sequence stratigraphy for explorationists and reservoir engineers. *Bulletin Centre de Recherche Exploitation-Production Elf Aquitaine Mem.* 25, 81 pp.

Howarth, V., Alves, T.M., 2016. Fluid flow through carbonate platforms as evidence for deep-seated reservoirs in Northwest Australia. *Marine Geology* 380, 17–43. <https://doi.org/10.1016/j.margeo.2016.06.011>

Jacquin, T., Dardeau, G., Durllet, C., de Graciansky, C., Hantzpergue, P., 1998. The north sea cycle: an overview of 2nd-order transgressive/regressive facies cycles in western europe, in: de Graciansky, P.-C., Hardenbol, J., Jacquin, T., Vail, P.R. (Eds.), *Mesozoic and Cenozoic Sequence Stratigraphy of European Basins*. SEPM Special Publication, pp. 445–466.

Jacquin, T., de Graciansky, P.-C., 1998. Major transgressive/regressive cycles: the stratigraphic signature of european basin development, in: De Graciansky, P.-C., Hardenbol, J., Jacquin, T., Vail, P.R. (Eds.), *Mesozoic and Cenozoic Sequence Stratigraphy of European Basins*. SEPM Special Publication, pp. 15–29.

Jorry, S.J., Bièvre, G., 2011. Integration of sedimentology and ground-penetrating radar for high-resolution imaging of a carbonate platform: High-resolution imaging of a carbonate platform. *Sedimentology* 58, 1370–1390. <https://doi.org/10.1111/j.1365-3091.2010.01213.x>

Kiessling, Wolfgang., Flügel, Erik., Golonka, Jan. (Eds.), 2002. *Phanerozoic Reef Patterns*. SEPM (Society for Sedimentary Geology). <https://doi.org/10.2110/pec.02.72>

Koša, E., 2015. Sea-level changes, shoreline journeys, and the seismic stratigraphy of Central Luconia, Miocene-present, offshore Sarawak, NW Borneo. *Marine and Petroleum Geology* 59, 35–55. <https://doi.org/10.1016/j.marpetgeo.2014.07.005>

Landrein, P., Vigneron, G., Delay, J., Lebon, P., Pagel, M., 2013. Lithologie, hydrodynamisme et thermicité dans le système sédimentaire multicouche recoupé par les forages Andra de Montiers-sur-Saulx (Meuse). *Bulletin de la Société Géologique de France* 184, 519–543. <https://doi.org/10.2113/gssgfbull.184.6.519>

Lathuilière, B., 2005. Introduction géologique à la carrière d'Ottange-Rumelange, in: *Fossiles et Minéraux de La Carrière d'Ottange-Rumelange*. pp. 15–25.

Lathuilière, B., 2000a. Reef building corals of Lower Bajocian of France (part 2). *Geobios* 33, 153–181.

Lathuilière, B., 2000b. Reef building corals of Lower Bajocian of France. Part 1. *Geobios* 33, 51–72.

Lathuilière, B., C., C., André, G., Dagallier, G., Durand, M., Hanzo, M., Huault, V., Harmand, D., Hibsich, C., Le Roux, J., Malartre, F., Martin-Garin, B., Nori, L., 2003. Production carbonatée dans le Jurassique de Lorraine. Presented at the Excursion, Groupe Français d'Etude du Jurassique.

Lathuilière, B., Marchal, D., 2009. Extinction, survival and recovery of corals from the Triassic to Middle Jurassic time. *Terra Nova* 21, 57–66. <https://doi.org/10.1111/j.1365-3121.2008.00856.x>

Loreau, J.P., Durllet, C., 1999. Diagenetic stratigraphy of discontinuity surfaces: an application to paleo-

environments and sequence stratigraphy. *Zentralblatt für Geologie und Paläontologie, Teil I Heft 3-4*, 381–407.

Macintyre, I.G., 1972. Submerged reefs of eastern Caribbean. *AAPG Bulletin* 56, 720–738.

Malikides, M., Harris, P.T., Jenkins, C.J., Keene, J.B., 1988. Carbonate sandwaves in Bass Strait. *Australian Journal of Earth Sciences* 35, 303–311. <https://doi.org/10.1080/08120098808729449>

Mancini, E.A., Blasingame, T.A., Archer, R., Panetta, B.J., Llinás, J.C., Haynes, C.D., Benson, D.J., 2004. Improving recovery from mature oil fields producing from carbonate reservoirs: Upper Jurassic Smackover Formation, Womack Hill field (eastern Gulf Coast, U.S.A.). *AAPG Bulletin* 88, 1629–1651. <https://doi.org/10.1306/06210404037>

Mangold, C., Poirot, E., Lathuilière, B., Le Roux, J., 1994. Biochronologie du Bajocien supérieur et du Bathonien de Lorraine (France). *Geobios M.S.* 17, 343–349.

Mari, J.L., Yven, B., 2014. The application of high-resolution 3D seismic data to model the distribution of mechanical and hydrogeological properties of a potential host rock for the deep storage of radioactive waste in France. *Marine and Petroleum Geology* 53, 133–153. <https://doi.org/10.1016/j.marpetgeo.2013.10.014>

Martín-Martín, J.D., Vergés, J., Saura, E., Moragas, M., Messenger, G., Baqués, V., Razin, P., Grélaud, C., Malaval, M., Jousseaume, R., 2017. Diapiric growth within an Early Jurassic rift basin: The Tazoult salt wall (central High Atlas, Morocco). *Tectonics* 36, 2–32.

Matyszkiewicz, J., Krajewski, M., Kędzierski, J., 2006. Origin and evolution of an Upper Jurassic complex of carbonate buildups from Zegarowe Rocks (Kraków–Wieluń Upland, Poland). *Facies* 52, 249–263. <https://doi.org/10.1007/s10347-005-0038-9>

Maubeuge, P.-L., 1956. Observations nouvelles sur l'Aalénien du Nord de Langres. *Bulletin technique des Mines de Fer de France* 3.

Nichol, S.L., Anderson, T.J., Battershill, C., Brooke, B.P., 2012. Submerged reefs and aeolian dunes as inherited habitats, Point Cloates, Carnarvon Shelf, Western Australia, in: *Seafloor Geomorphology as Benthic Habitat*. Elsevier, pp. 397–407.

Olivier, N., Lathuilière, B., Thiry-Bastien, P., 2006. Growth models of Bajocian coral-microbialite reefs of Chargey-les-Port (eastern France): palaeoenvironmental interpretations. *Facies* 52, 113–127. <https://doi.org/10.1007/s10347-005-0022-4>

Olivier, N., Pittet, B., Gaillard, C., Hantzpergue, P., 2007. High-frequency palaeoenvironmental fluctuations recorded in Jurassic coral- and sponge-microbialite bioconstructions. *Comptes Rendus Palevol* 6, 21–36. <https://doi.org/10.1016/j.crpv.2006.07.005>

Olivier, N., Pittet, B., Werner, W., Hantzpergue, P., Gaillard, C., 2008. Facies distribution and coral-microbialite reef development on a low-energy carbonate ramp (Chay Peninsula, Kimmeridgian, western France). *Sedimentary Geology* 205, 14–33. <https://doi.org/10.1016/j.sedgeo.2007.12.011>

Pagel, M., 2014. Introduction to present and past transfers in a sedimentary aquifer–aquitard system: A 2000 m deep drill-hole in the Mesozoic of the Paris Basin. *Marine and Petroleum Geology* 53, 1–2. <https://doi.org/10.1016/j.marpetgeo.2014.02.008>

Pagel, M., Bonifacie, M., Schneider, D.A., Gautheron, C., Brigaud, B., Calmels, D., Cros, A., Saint-Bezar, B., Landrein, P., Sutcliffe, C., Davis, D., Chaduteau, C., 2018. Improving paleohydrological and diagenetic reconstructions in calcite veins and breccia of a sedimentary basin by combining $\Delta 47$ temperature, $\delta 18\text{O}_{\text{water}}$ and U-Pb age. *Chemical Geology* 481, 1–17. <https://doi.org/10.1016/j.chemgeo.2017.12.026>

Piuz, A.D., 2008. Associations micro-faunistiques de la plate-forme échinodermique bajocienne du Jura et de Bourgogne: Implications paléoenvironnementales. *Archive des Sciences* 120–128.

Pomar, L., 2001. Types of carbonate platforms: a genetic approach. *Basin Research* 13, 313–334. <https://doi.org/10.1046/j.0950-091x.2001.00152.x>

Pomar, L., 1991. Reef geometries, erosion surfaces and high-frequency sea-level changes, upper Miocene Reef Complex, Mallorca, Spain. *Sedimentology* 38, 243–269. <https://doi.org/10.1111/j.1365-3091.1991.tb01259.x>

Poprawski, Y., Basile, C., Jaillard, E., Gaudin, M., Lopez, M., 2016. Halokinetic sequences in carbonate systems: An example from the Middle Albian Bakio Breccias Formation (Basque Country, Spain). *Sedimentary Geology* 334, 34–52. <https://doi.org/10.1016/j.sedgeo.2016.01.013>

Rankey, E.C., Reeder, S.L., 2012. Tidal Sands of the Bahamian Archipelago, in: Davis, R.A., Dalrymple, R.W. (Eds.), *Principles of Tidal Sedimentology*. Springer Netherlands, Dordrecht, pp. 537–565. https://doi.org/10.1007/978-94-007-0123-6_20

Rankey, E.C., Riegl, B., Steffen, K., 2006. Form, function and feedbacks in a tidally dominated ooid shoal, Bahamas. *Sedimentology* 53, 1191–1210.

Rebours, H., André, G., Cruchaudet, M., Dewonck, S., Distinguin, M., Drouiller, Y., Robin, P., Wileveau, Y., Delay, J., 2004. Forages de reconnaissance de la formation - Synthèse FRF - Laboratoire de recherche souterrain de Meuse/Haute-Marne - Volume I texte (No. D RP ADPE 04 1245). Andra.

Reynaud, J.-Y., Dalrymple, R.W., 2012. Shallow-Marine Tidal Deposits, in: Davis, R.A., Dalrymple, R.W. (Eds.), *Principles of Tidal Sedimentology*. Springer Netherlands, Dordrecht, pp. 335–369. https://doi.org/10.1007/978-94-007-0123-6_13

Riera, R., Lebec, U., Lang, S.C., Paumard, V., 2023. Differentiating reefal ridges from relict coastal ridges: Lessons from the seismic geomorphologic study of buried Miocene buildups (North West Shelf, Australia). *Basin Research* 35, 1793–1814. <https://doi.org/10.1111/bre.12774>

Schlager, W., Purkis, S., 2015. Reticulate reef patterns—antecedent karst versus self-organization. *Sedimentology* 62, 501–515.

Teixell, A., Barnolas, A., Rosales, I., Arboleya, M.-L., 2017. Structural and facies architecture of a diapir-related carbonate minibasin (lower and middle Jurassic, High Atlas, Morocco). *Marine and Petroleum Geology* 81, 334–360.

Teyssen, T.A.L., 1984. Sedimentology of the Minette oolitic ironstones of Luxembourg and Lorraine: a Jurassic subtidal sandwave complex. *Sedimentology* 31, 195–211. <https://doi.org/10.1111/j.1365-3091.1984.tb01959.x>

Thiry-Bastien, P., 2002. Stratigraphie séquentielle des calcaires bajociens de l'Est de la France (Jura-Bassin de Paris)

(PhD thesis). Université Claude Bernard, Lyon.

Todd, B.J., Shaw, J., 2009. International year of planet earth 5. Applications of seafloor mapping on the Canadian Atlantic continental shelf. *Geoscience Canada* 36, 81–94.

Vennin, E., Boisseau, T., Proust, J.-N., Chuvashov, B.I., 2003. Influence of Eustasy and Tectonism on Reef Architecture in Early Permian Reef Complexes, Southern Urals, Russia, in: Zempolich, W.G., Cook, H.E. (Eds.), *Paleozoic Carbonates of the Commonwealth of Independent States (CIS): Subsurface Reservoirs and Outcrop Analogs*, SEPM Special Publication. SEPM Society for Sedimentary Geology. <https://doi.org/10.2110/pec.02.74.0205>

Vennin, E., Bouton, A., Roche, A., Gérard, E., Bundeleva, I., Boussagol, P., Wattinne, A., Kolodka, C., Gaucher, E., Virgone, A., Visscher, P.T., 2021. The Limagne Basin: a journey through modern and fossil microbial deposits. *BSGF - Earth Sci. Bull.* 192, 41. <https://doi.org/10.1051/bsgf/2021030>

Vennin, E., Rouchy, J.-M., Chaix, C., Blanc-Valleron, M.-M., Caruso, A., Rommevau, V., 2004. Paleocological constraints on reef-coral morphologies in the Tortonian–early Messinian of the Lorca Basin, SE Spain. *Palaeogeography, Palaeoclimatology, Palaeoecology* 213, 163–185.

Vincent, B., 2001. *Sédimentologie et Géochimie de la Diagenèse des carbonates. Application au Malm de la bordure Est du Bassin de Paris* (PhD Thesis). University of Burgundy, Dijon.

Vincent, B., Brigaud, B., Thomas, H., Gaumet, F., 2021. Giant subaqueous carbonate dunes: a revised interpretation of large-scale oo-bioclastic clinofolds in the middle Jurassic of the Paris Basin and its implications. *Facies* 67, 12. <https://doi.org/10.1007/s10347-021-00621-4>

Vincent, B., Emmanuel, L., Houél, P., Loreau, J.-P., 2007. Geodynamic control on carbonate diagenesis: Petrographic and isotopic investigation of the Upper Jurassic formations of the Paris Basin (France). *Sedimentary Geology* 197, 267–289. <https://doi.org/10.1016/j.sedgeo.2006.10.008>

Wolpert, P., Aigner, T., Bendias, D., Beichel, K., Zosseder, K., 2022. A novel workflow for geothermal exploration: 3D seismic interpretation of biohermal buildups (Upper Jurassic, Molasse Basin, Germany). *Geotherm Energy* 10, 27. <https://doi.org/10.1186/s40517-022-00235-1>

Zeyen, H., Léger, E., 2024. PyRefra – Refraction seismic data treatment and inversion. *Computers & Geosciences* 185, 105556. <https://doi.org/10.1016/j.cageo.2024.105556>

10. Figure Captions

Figure 1: A- Paleogeographic map (late Jurassic) from R. Blakey's maps, <https://deeptimemaps.com>. B- Paleogeographic map (Callovian) from Atlas Peri-Tethys (Dercourt et al., 2000). C-D- Geological maps with the location of the Andra Underground Research Laboratory (URL) site and associated wells and seismic surveys, and positioning all the studied outcrop sections.

Figure 2: A- Log of the EST-433 borehole, with calibration of the main formation/member tops on a regional 2D seismic line. B- Lithostratigraphy at regional scale along a N-S trend between the EST-433 and Audun-le-Roman 101 boreholes.

Figure 3: Early Bajocian outcrop photographs and thin section photomicrographs illustrating facies variability. A- View of Attignéville quarry showing the carbonate succession from the *Marnes micacées* Mb to the *Marnes de Longwy* Fm. B- Silty claystone and marls (facies F1a) and bioclastic packstone or grainstone alternations (facies F1c) in Rouvres-la-Chétive quarry. C- Marls and bioclastic packstone or grainstone alternations (facies F1c) in Attignéville quarry, showing hummocky-cross stratification (location of AT1 sample of Fig. 3F is marked). D- Zoom on HCS in the marls and bioclastic packstone or grainstone alternations (facies F1c) in Attignéville quarry. E- Packstone to grainstone (facies F1b, Attignéville quarry, sample AT8), composed of echinoderms (ech), nubecularia (nu) oncoids (on), ooids (oo), and superficial ooids (s. oo) with late sparite cement. This facies is found in marl-limestone alternations where limestone beds are tens of meters thick. F- Bioclastic packstone to grainstone alternations (facies F1c, *Calcaires à entroques*, Attignéville quarry, sample AT1), composed of echinoderms (ech), crinoids (cri), and detrital quartz (qz) cemented by sparite and altered Fe-rich dolomite. This facies is found in marl-limestone alternations where limestone beds are tens of centimeters thick and contain HCS. G- A boundstone with recrystallized branching corals (br.) in a muddy and micro-bioclastic matrix (facies F2a, *Calcaire à Polypiers inférieur*, borehole EST210, sample E160, measured depth of 1079 m). H- Bioclastic grainstone (facies F2c, *Oolithes à Clypeus angustiporus*, Rouvres-la-Chétive quarry, sample Rou3), composed of

coral fragments, echinoderms (ech), crinoids (cri), and bryozoans (bryo). Note the early cementation (ec) consisting of isopachous bladed cements.

Figure 4: Sequence stratigraphy correlation between the key outcrop sections.

Figure 5: A- Photograph of the lower part of the *Calcaires à Polypiers* Formation, Attignéville quarry. B- Sketch from photo A showing the facies and lithostratigraphic units. C- Electrical resistivity tomography profile (ERT profile1) with facies interpretations (see discussion in the text). D- FDEM profile with facies interpretations (see discussion in the text).

Figure 6: A- Photograph of the lower part of the *Calcaires à Polypiers* Formation in Beaufremont quarry, showing a coral bioherm. All locations of near-surface resistivity and GPR acquisition profiles are indicated. B- Sketch from photo A with interpreted facies. C- GPR profile 6 acquired on the top floor of the quarry with interpreted facies; the chaotic reflectors illustrate the bioherm, with onlaps and pinch-outs on its edges (arrows). D- Electrical resistivity tomography profile (ERT profile 2) acquired on the top floor of the quarry (see discussion in the text). E- Electrical resistivity tomography profile (ERT profile 3) acquired on the ground floor of the quarry, in front of the main faces of photo A (see discussion in the text).

Figure 7: A- Photograph of the *Calcaires à Polypiers inférieurs*, *Oncolithe cannabine* and *Calcaires à Polypiers supérieurs* members in Beaufremont quarry, showing the top of a coral bioherm at the base of another face than Figure 6. B- Sketch from photo A with facies interpretation. C- Electrical resistivity tomography profile 4 acquired on the ground floor in front of the face (see discussion in the text). D- FDEM profile 2 acquired on the ground floor in front of the face (see discussion in the text). E- GPR profile 14 acquired on the ground floor in front of the face; note the chaotic reflectors of the bioherm (orange) and the parallel continuous reflectors of the facies infilling the topography adjacent to the bioherm (green).

Figure 8: A- Location on the Beaufremont quarry satellite photo of the three electrical resistivity tomography (ERT) profiles ERT2, ERT3, ERT4, the frequency-domain electromagnetic (FDEM) profile FDEM2, the two ground penetrating radar (GPR) profiles GRP6, GPR14, and the seismic profile S1. The two panoramas illustrated in Figure 6 and Figure 7 are also indicated. B- NW–SE seismic profile S1 acquired on the ground floor of Beaufremont quarry revealing three patches of high velocity, A, B, and C, between 1 m and 6 m below the surface; note the trough of low velocity between patches A and B.

Figure 9: A- NE–SW panoramic view of Rouvres-la-Chétive quarry B- Sketch from photo A with facies interpretation. C- Focus on the SW corner of the quarry showing a coral bioherm installed on top of large cross beds of the *Oolithe à Clypeus angustiporus*; the crest of the cross beds is oriented N120° and the main dip direction of the sets is N30°. D/E- Zoom on the same corner showing the slope of the sets of the large cross beds capped by a hardground with annelid perforation (perf.) in thin section photo E; the facies of the *Oncolithe cannabine* fill the topography in front of the bioherm and cross beds. F- NW–SE panoramic view of the quarry showing lower angle slopes of the sets of cross beds, with a bioherm installed on top. G- Sketch from photo F with facies interpretation.

Figure 10: A- Location on the Rouvres-la-Chétive quarry satellite photo of the seismic profiles S3 and S4 and of the two panoramas, illustrated in Figure 9 for comparison. B- SW–NE seismic profile acquired behind a face of Rouvres-la-Chétive quarry and showing a boundary of velocity contrast, first slightly dipping from SW to NE and plunging towards the NE between 45 m and 55m (dotted line). C- N–S seismic profile acquired slightly farther behind the same face of Rouvres-la-Chétive quarry, also revealing the same boundary of velocity contrast although in a more complex arrangement (see dotted line and the text for explanation).

Figure 11: A- Location on the Sommerécourt quarry satellite photo of electrical resistivity tomography (ERT) profile ERT5, the frequency-domain electromagnetic (FDEM) profile FDEM5, the ground penetrating radar (GPR) profile GRP2 and seismic profile S2, and the

panoramas. B- 3D block diagram of Sommerécourt quarry displaying the possible N120° orientation of the coral ridge. C-D- Large-scale panoramic view and facies-interpreted sketch of Sommerécourt quarry showing large coral bioherms; troughs between bioherms are filled with well-bedded facies, including some products of dismantling of bioherms, see eye in A for location of the observation point. E-F- Second panoramic view and facies-interpreted sketch of Sommerécourt quarry, from another observation point (see eye in A for location of the observation point). The coral bioherms high is oriented N120°.

Figure 12: A- Facies-interpreted sketch of photo C of Figure 11, Sommerécourt quarry. B- GPR profile 2 acquired on the intermediate floor of the quarry (aligned blocks of rocks in photo A); note the clear imaging of bioherms with chaotic reflectors (orange), and the more parallel reflectors of the sediments filling the inter-bioherm trough (yellow and green). C- FDEM profile 5 acquired on the ground floor of the quarry (see discussion in the text). D- Seismic profile 2 acquired on the ground floor of the quarry; velocities increase with depth, but an undulation of the top of the high-velocity zone (>4 km/s) is visible (see discussion in the text). E- Electrical resistivity tomography profile 5 acquired on the ground floor of the quarry (see discussion in the text). F- Facies-interpreted sketch of photo A, extended into shallow subsurface by an interpretation of near-surface geophysical results (0 m is the ground floor of the quarry).

Figure 13: A- Dip attribute maps from 3D seismic image extracted on Top Dogger. B- Dip attribute maps from 3D seismic image revealing some elongated N120° structures on the top of the *Calcaires à Polypiers* Formation. C- Azimuthal dip attribute map at the top of the *Calcaires à Polypiers* Formation; the main dip direction of the N120° structures is NE. D- Isochron map of the *Calcaires à Polypiers* Formation; the N120° structures correspond to thicker time intervals.

Figure 14: A- Well logs of the EST-210 borehole with a vertical seismic profile (VSP) illustrating positive features in the *Calcaires à Polypiers* Formation. B- Crossline 255 (2010 3D seismic)

and trajectories of EST-210, EST-211, and EST-212 boreholes; the red interval is the cored interval in EST-210 (section in D). C- Close-up of the VSP of the EST-210 well showing that the positive features are situated in the lower part of the *Calcaires à Polypiers* Formation. D- Sedimentological log of the cored section of the EST-210 borehole with sonic log and P-wave velocities on core plug samples (Brigaud et al., 2010).

Figure 15: A- Sketch of the early Bajocian platform sedimentary architectures, built from the direct and indirect (near-surface geophysics) observations in various outcrops; two main seismic reflectors correspond to the base and top of the *Calcaires à Polypiers* Formation, but internal architectures are below the resolution. B- Isochron map of the *Calcaires à Polypiers* Formation, with contouring of the N120° elongated biohermal ridges. C- Interpretation of the isochron map in terms of facies; biohermal ridges are more massive and interfingered than previously thought on the basis of the small 1999 URL bloc to the S.

Figure 16: A- Crossline 270 (2010 3D seismic) illustrating the undulating aspect of the top reflector of the *Calcaires à Polypiers* Formation. B- Zoom on the Bajocian/Bathonian interval showing that the positive features responsible for the undulation of the top reflector are situated at the base of the formation (coral patches). C- Same profile with interpreted coral patches; the upper half of the *Calcaires à Polypiers* Formation exhibits continuous parallel reflectors, levelling the topography.

Figure 17: A- Satellite view of part of the Great Bahama Bank showing a large shoal complex with giant tidal carbonate sand dunes (image Landsat 2014). B- Zoom on the eastern part of the shoal complex showing longitudinal dunes and bathymetries available at <https://map.openseamap.org/>. C- Dip attribute map from 3D seismic image at the top of the *Calcaires à Polypiers* Formation, rescaled as in B (see the text for comparison and discussion).

Figure 18: Conceptual sketch of development and evolution of the Bajocian carbonate platform, illustrating the variations of some key controlling factors on the carbonate

factory(ies). Topographic undulations were created in the early stages of the platform with migrating giant subaqueous dunes that served as nucleation points for the growth of coral bioherms; the undulations were levelled progressively as the platform evolved.

PREPRINT



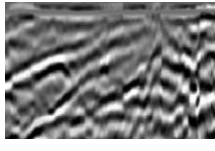
Depositional environment	Facies	Grains 1- Non-skeletal 2- Skeletal	Sedimentary and biogenic structures	Ground Penetrating Radar (GPR)	Resistivities for Electrical Resistivity Tomography (ERT) and frequency-domain electromagnetics (FDEM); Seismic velocities (S)
Mid ramp Storm-dominated environment (Facies Association FA1)	Facies F1a – Silty claystone to siltstone	1- Silt-sized quartz (C) 2- Bivalves (R)	Storm-graded layers Bioturbations (<i>Planolites</i>)		ERT: 30–500 Ohm.m FDEM: 10–70 Ohm.m
	Facies F1b – Marls and oncoidal packstone or grainstone alternations	1- Oncoids (C/F), superficial ooids / peloids(R), silt-sized quartz (C) 2- Echinoderms (F), bivalves (F), brachiopods (R), bryozoans (R)	Storm-graded layers Rare bioturbations		ERT: 200–800 Ohm.m FDEM: 300–1100 Ohm.m S: 1–1.8 km.s-1
	Facies F1c – Marls and bioclastic packstone or grainstone alternations	1- Silt to sand-sized quartz (C), peloids (C) 2- Echinoderms (F), bivalves (F), brachiopods (R)	Storm-graded layers Hummocky-cross stratification		ERT: 300–1000 Ohm.m EM: 50–400 Ohm.m
Inner ramp high energy Shoal environment Ooid/peloid or skeletal-dominated facies (Facies Association FA2)	Facies F2a – Coral bioconstructions	1- Peloids (R/C), intraclasts (R) 2- Platy colonies, predominantly <i>Isastrea</i> genus (A), branching colonies (branching phaceloid) (C), crinoids (C), microbial encrustations (C), bivalves (R), gastropods (R), bryozoans (R)	Dome-shaped bioherms or lens-shaped biostromes		ERT: 600–2000 Ohm.m EM: 400–1000 Ohm.m S: 2–3 km.s-1 at Beaufremont and Rouvres-la-Chétive 4–5 km.s-1 at Sommerécourt
	Facies F2b - Bioclastic grainstone to rudstone	1-Peloids (A), oncoids (R/C), intraclasts (R) 2-Bivalves (A), coral fragments (A), echinoderms (C), bryozoans (C), brachiopods (C), gastropods (R), serpulids (R)	Sigmoidal crossbedding		ERT: 500–1200 Ohm.m S: 3–3.5 km.s-1
Possible inner to mid ramp transition	Facies F2c -Cross-bedded peloidal/oolitic and bioclastic grainstone	1-Superficial ooids (C), peloids (F) 2-Echinoderms (C), bivalves (A), bryozoans (C), coral fragments (F)	Large scale crossbedding		S: 4–5 km.s-1

Table 1: Facies descriptions, facies associations, and interpretation of depositional environments.

R = Rare <10%; C = Common 10–20%; F = Frequent 20–50%; A = Abundant >50%.

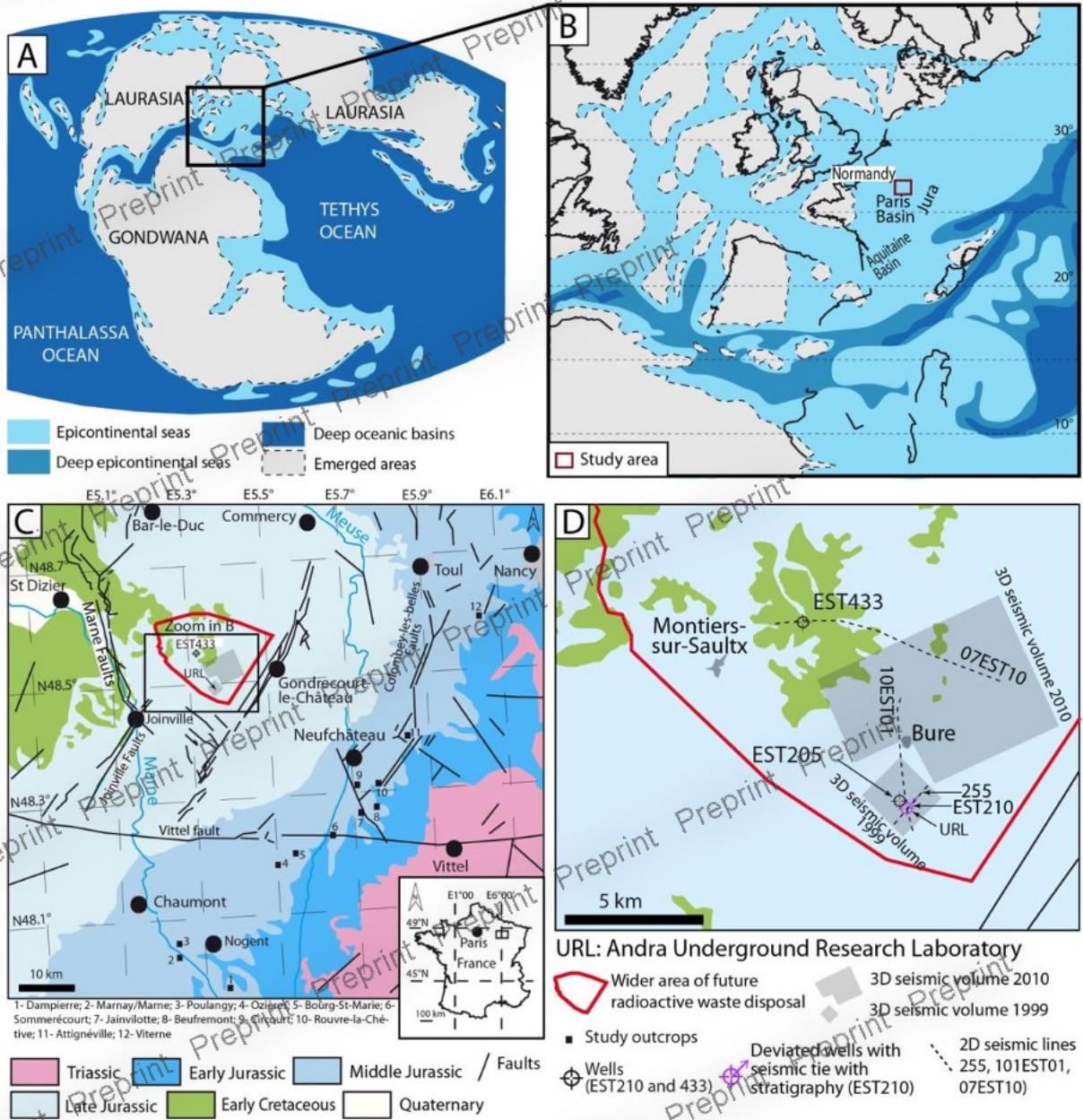


Fig. 1

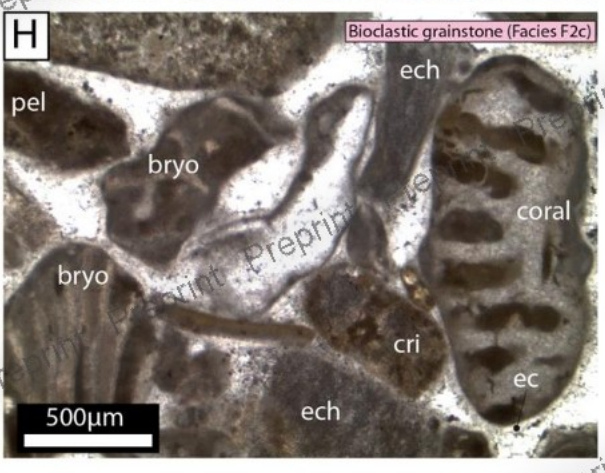
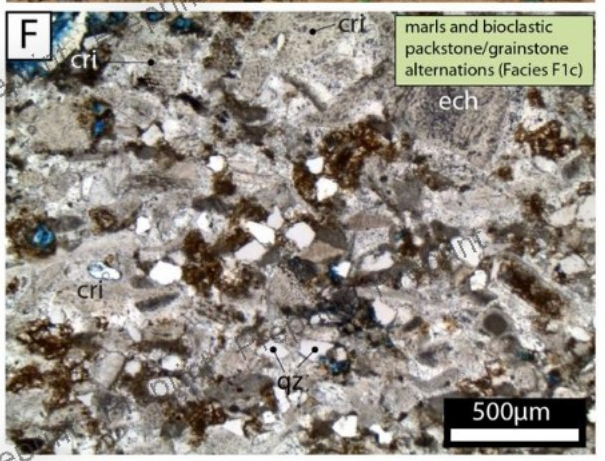
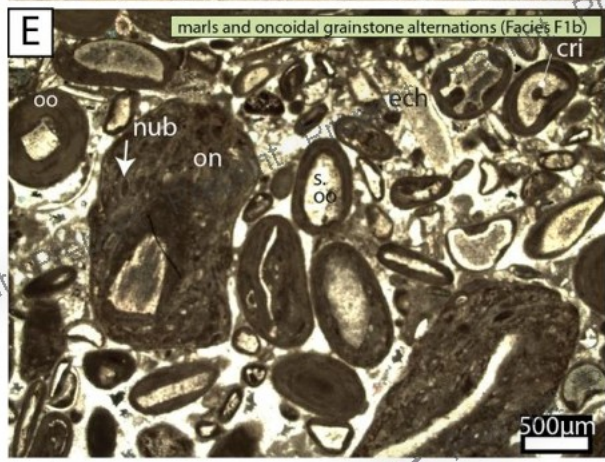
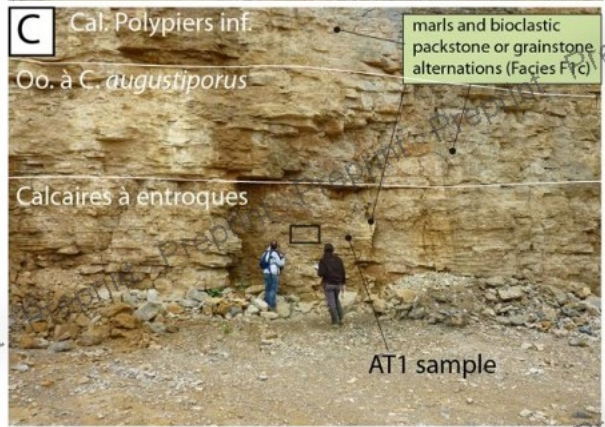
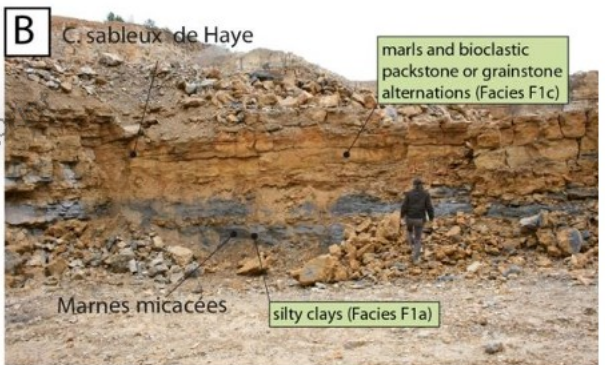
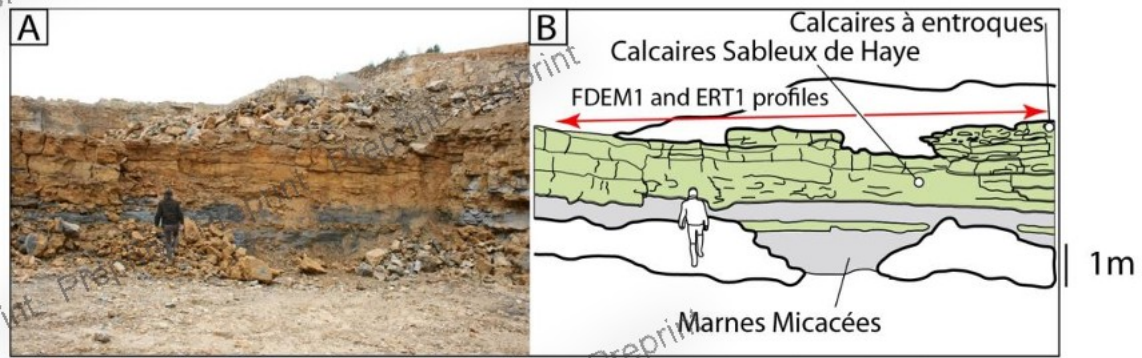


Fig. 3



Marls and bioclastic packstone or grainstone alternations - Mid ramp (facies F1c)
 Silty claystone to siltstone (facies F1a) Mid ramp (facies F1a)

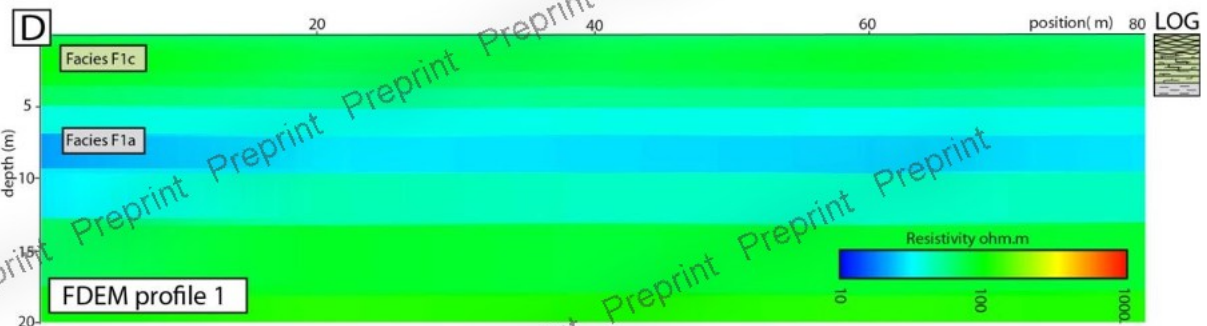
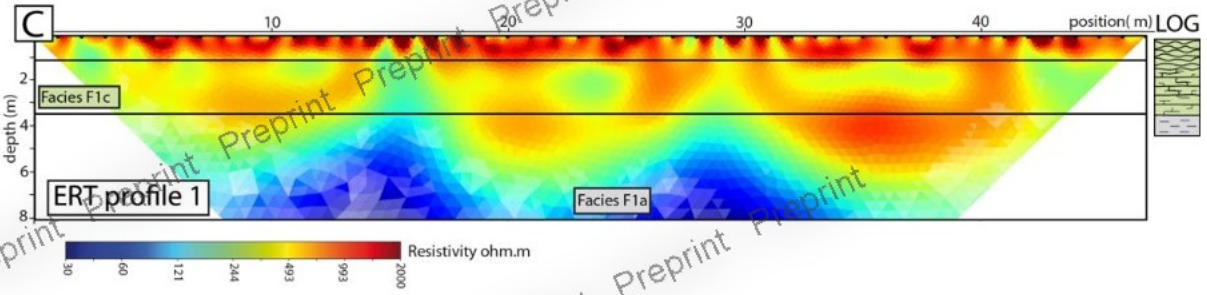


Fig. 5

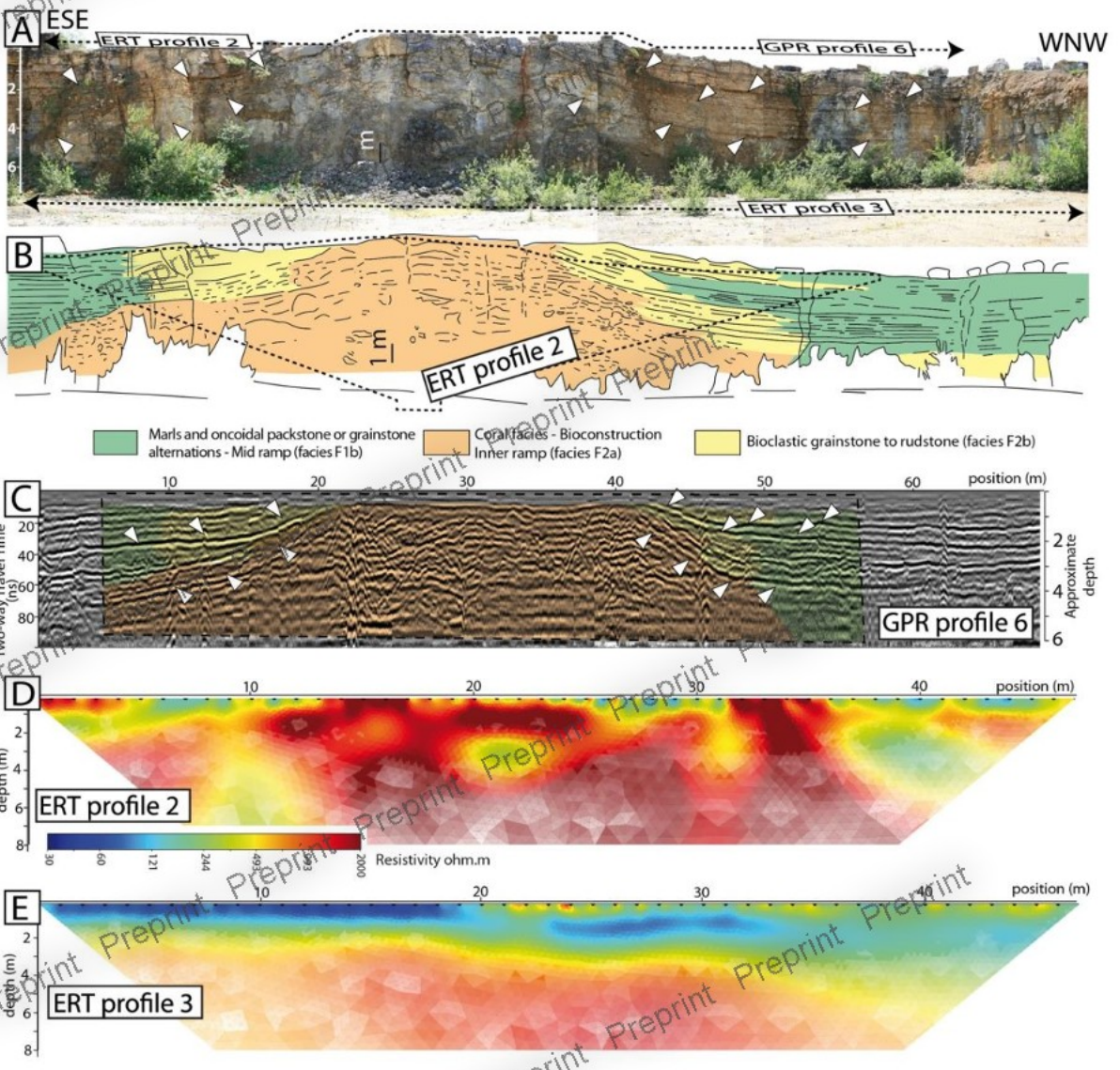


Fig. 6

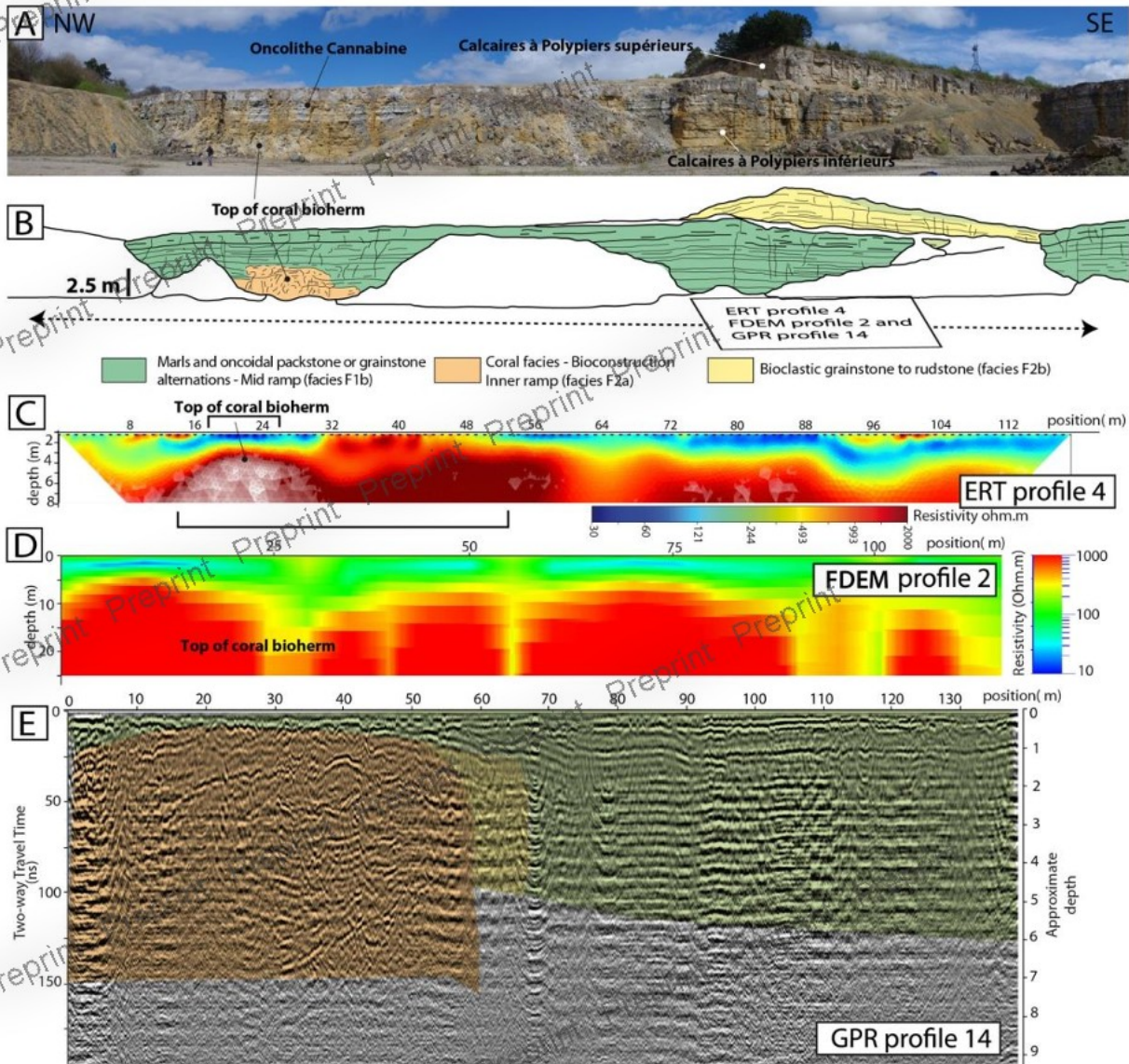


Fig. 7

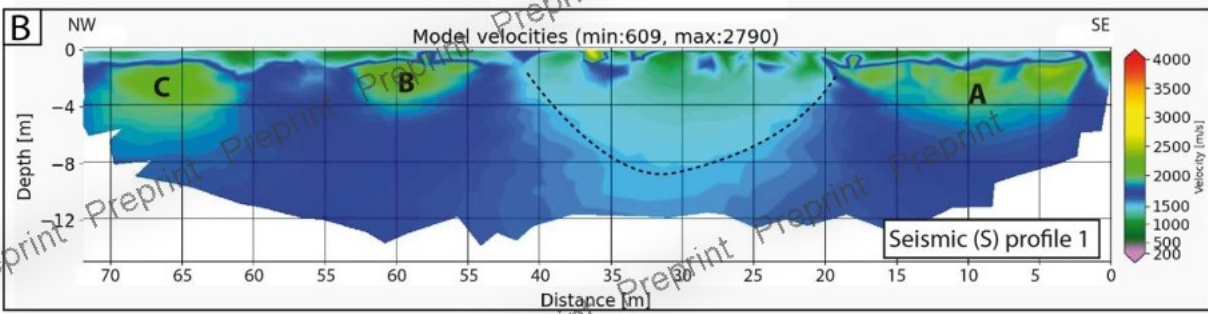
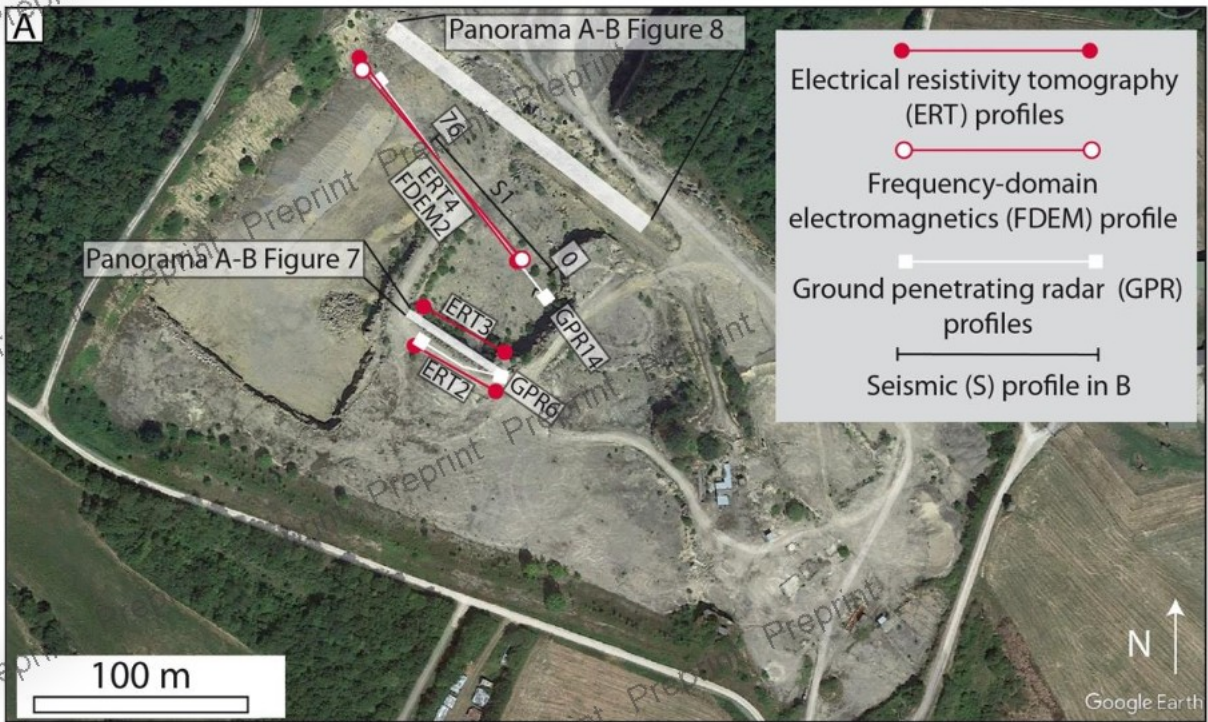


Fig. 8

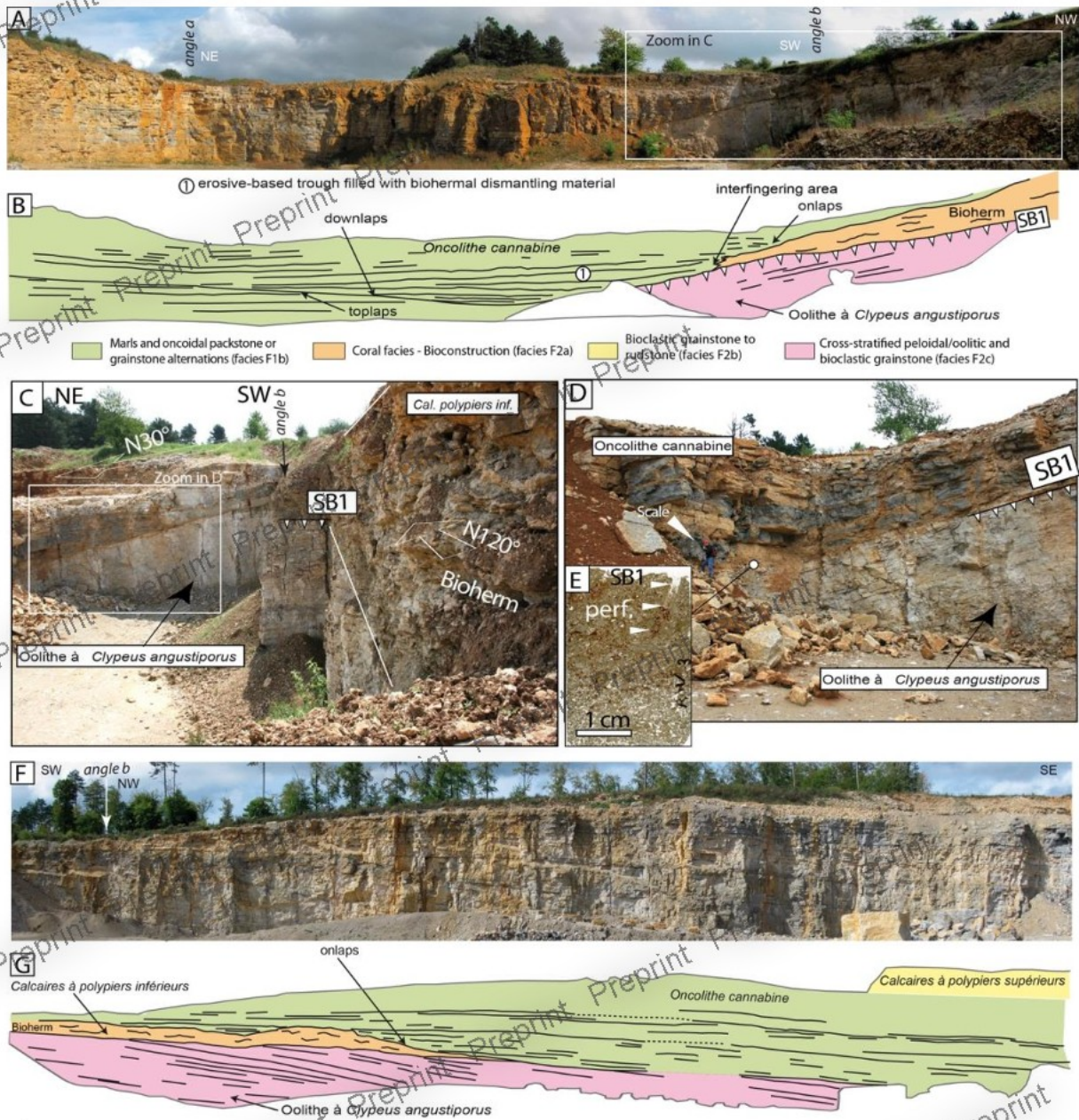


Fig. 9

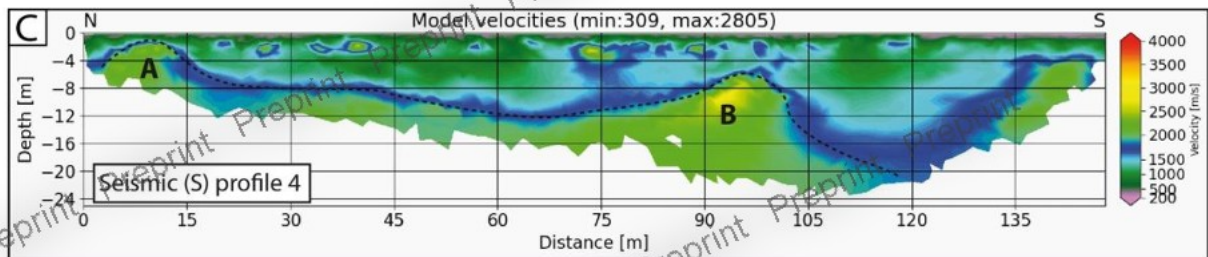
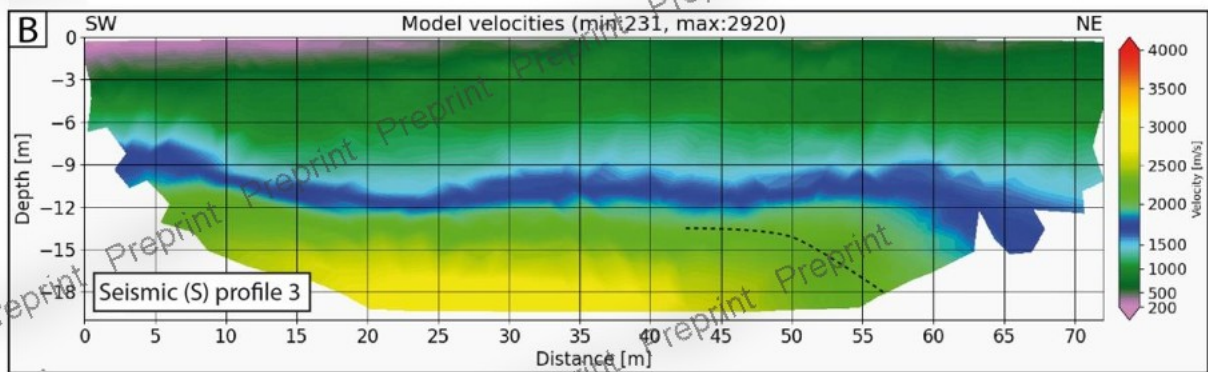
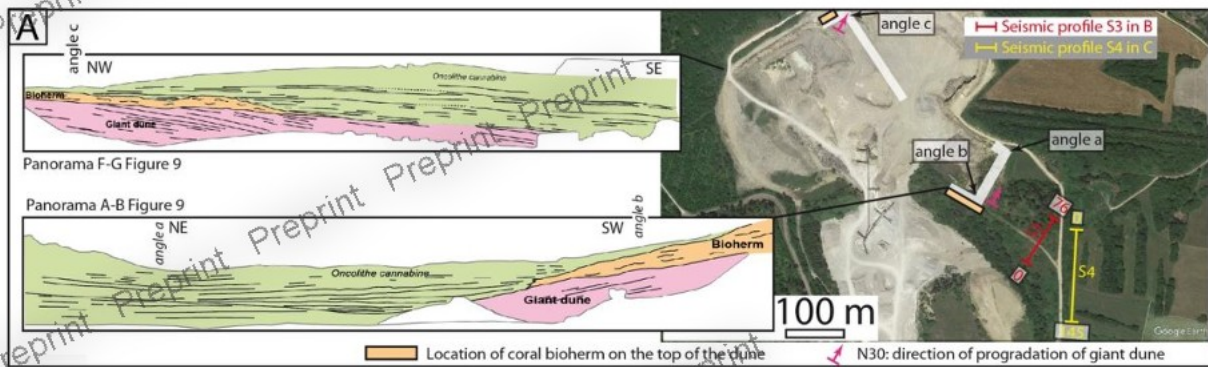
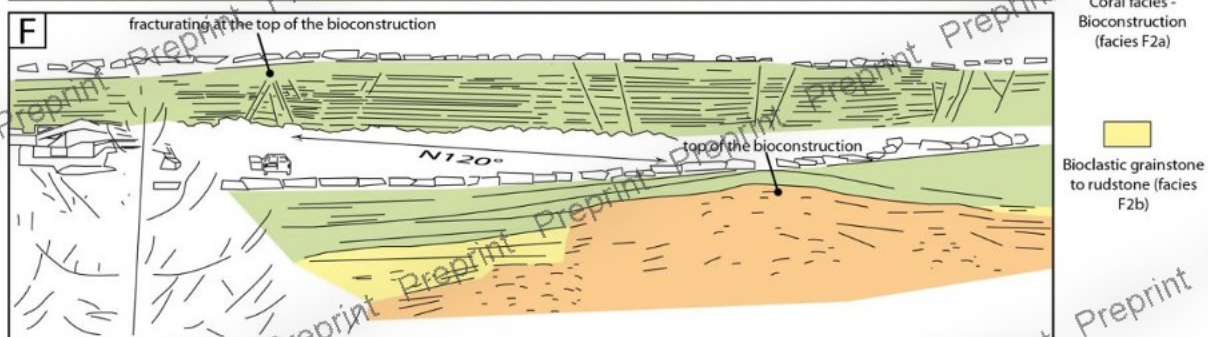
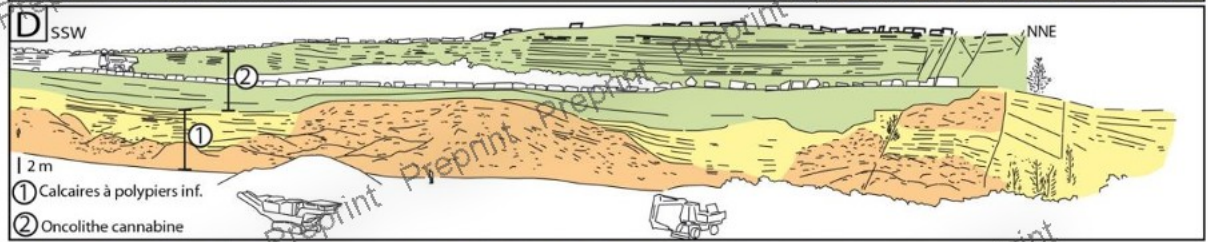
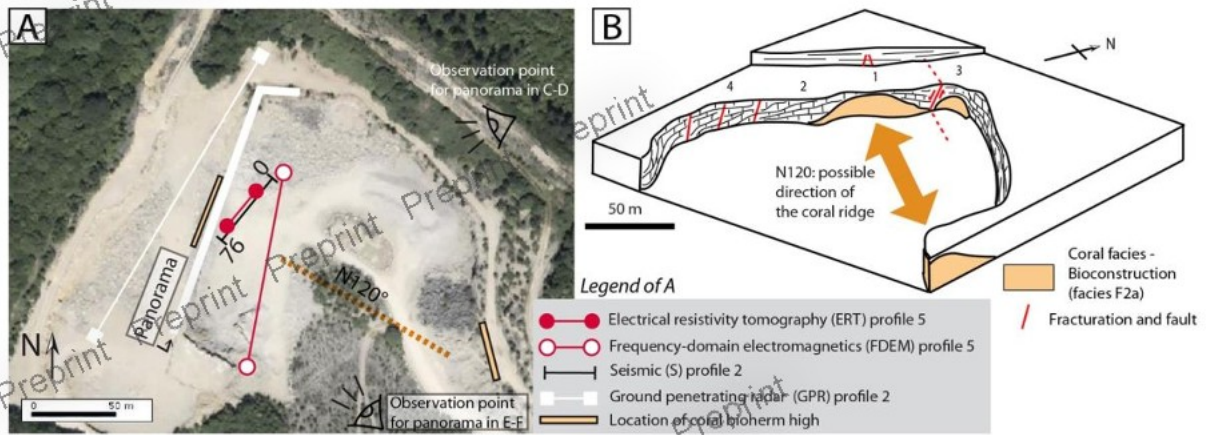


Fig. 10



- Marls and oncoidal packstone or grainstone alternations (facies F1b)
- Coral facies - Bioconstruction (facies F2a)
- Blastic grainstone to rudstone (facies F2b)

Fig. 11

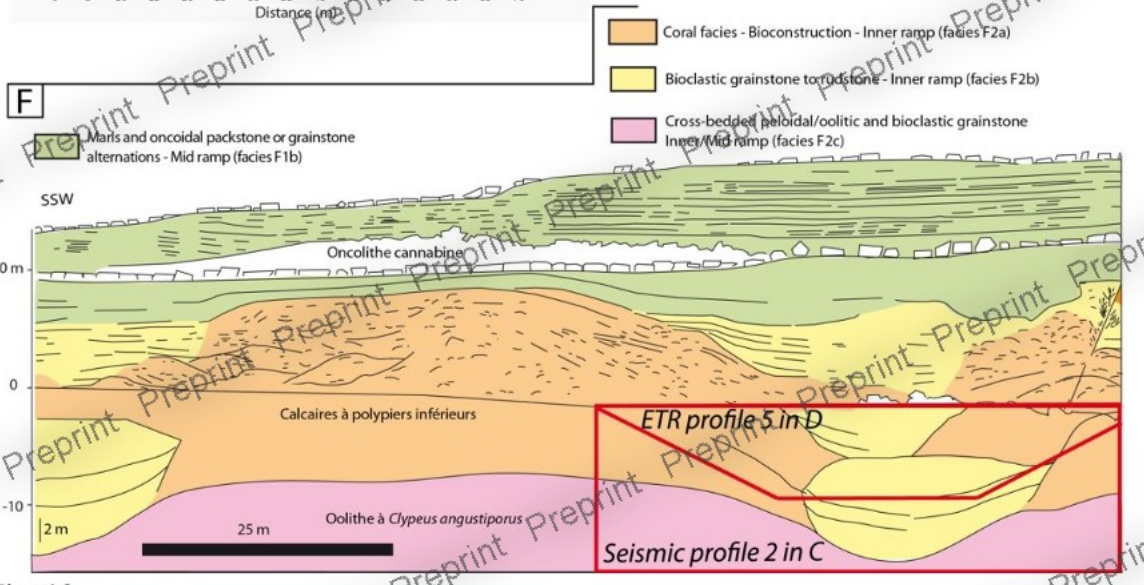
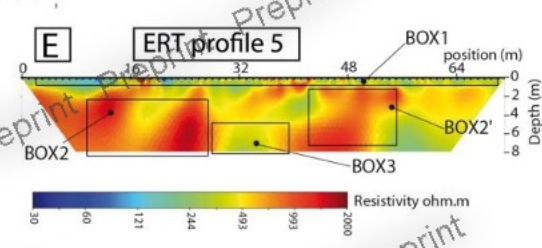
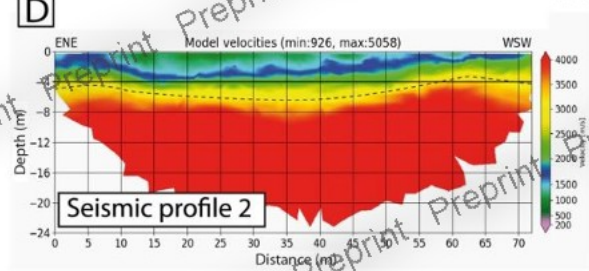
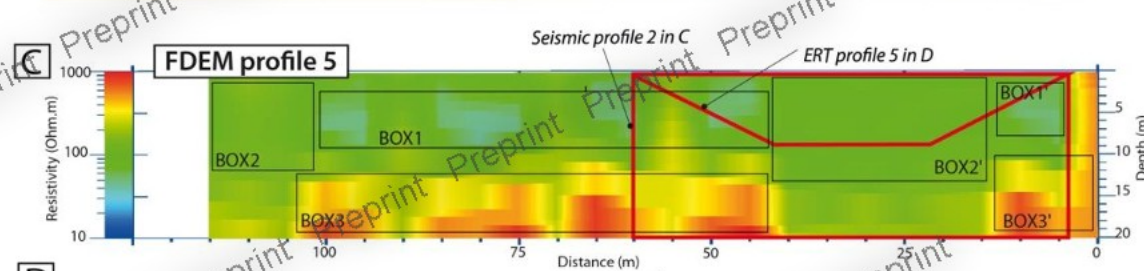
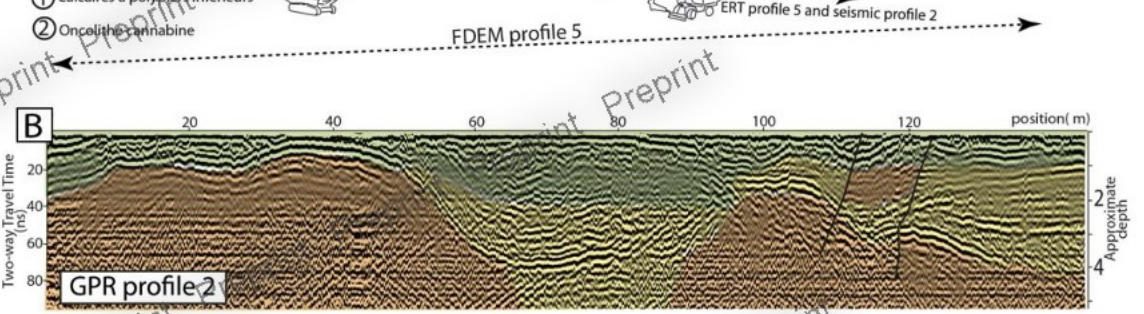
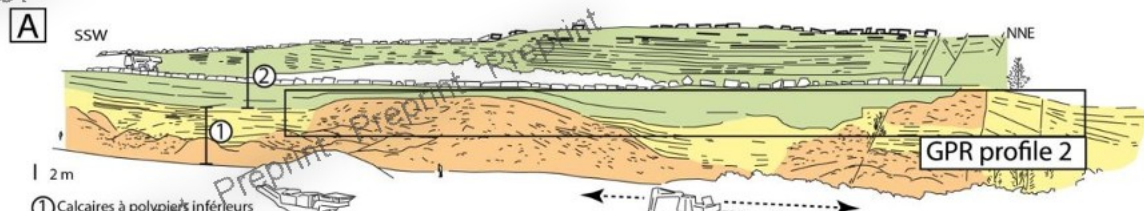


Fig. 12

Preprint Preprint Preprint Preprint

A- Dip attribute map extracted on Top Dogger

B- Dip attribute map extracted on Top of Calc. à Polypiers Fm.

C- Azimuthal dip attribute map extracted at the top of the Calcaires à Polypiers Fm.

D- Isochron map of the Calcaires à Polypiers Fm.

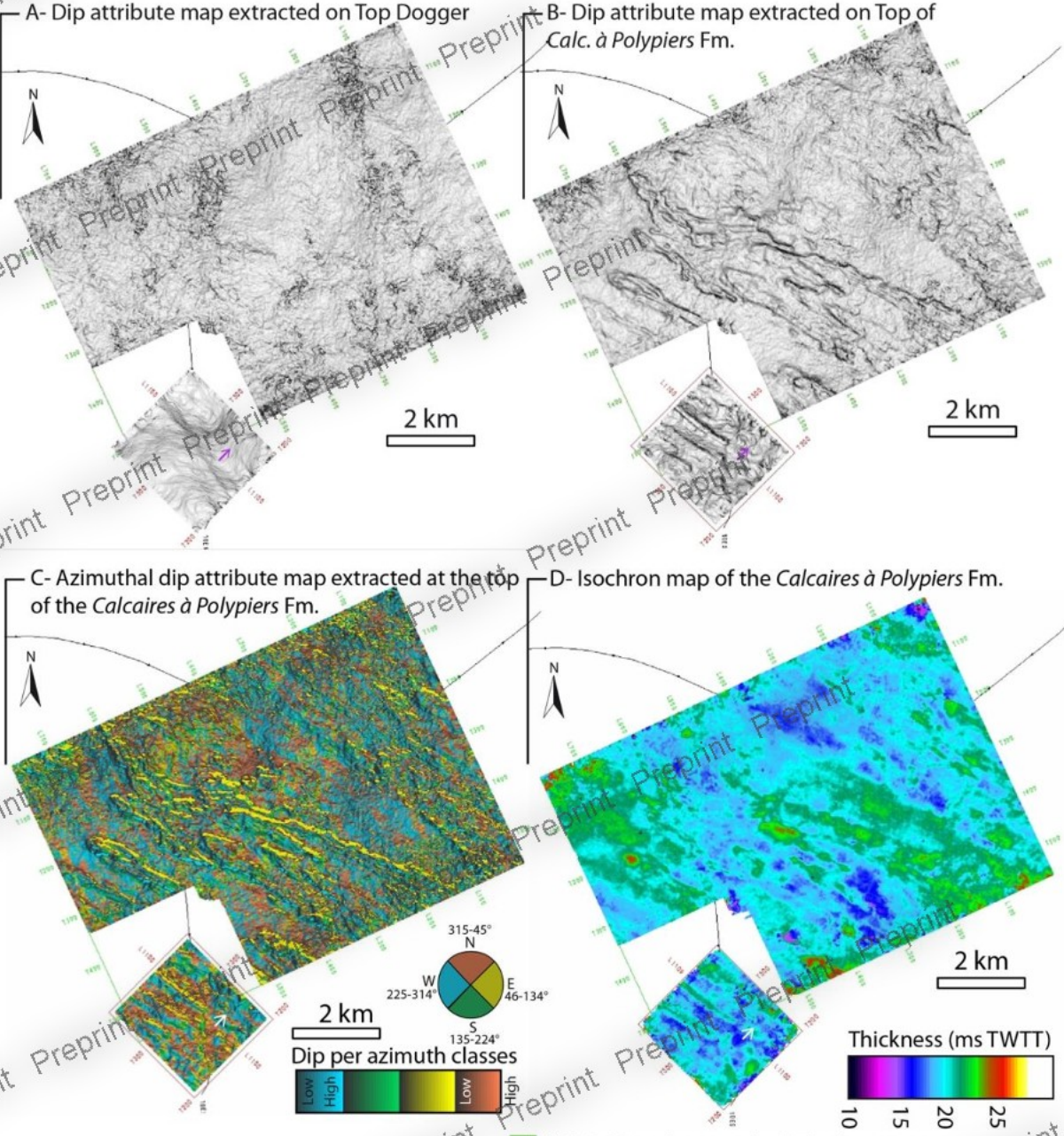


Fig. 13

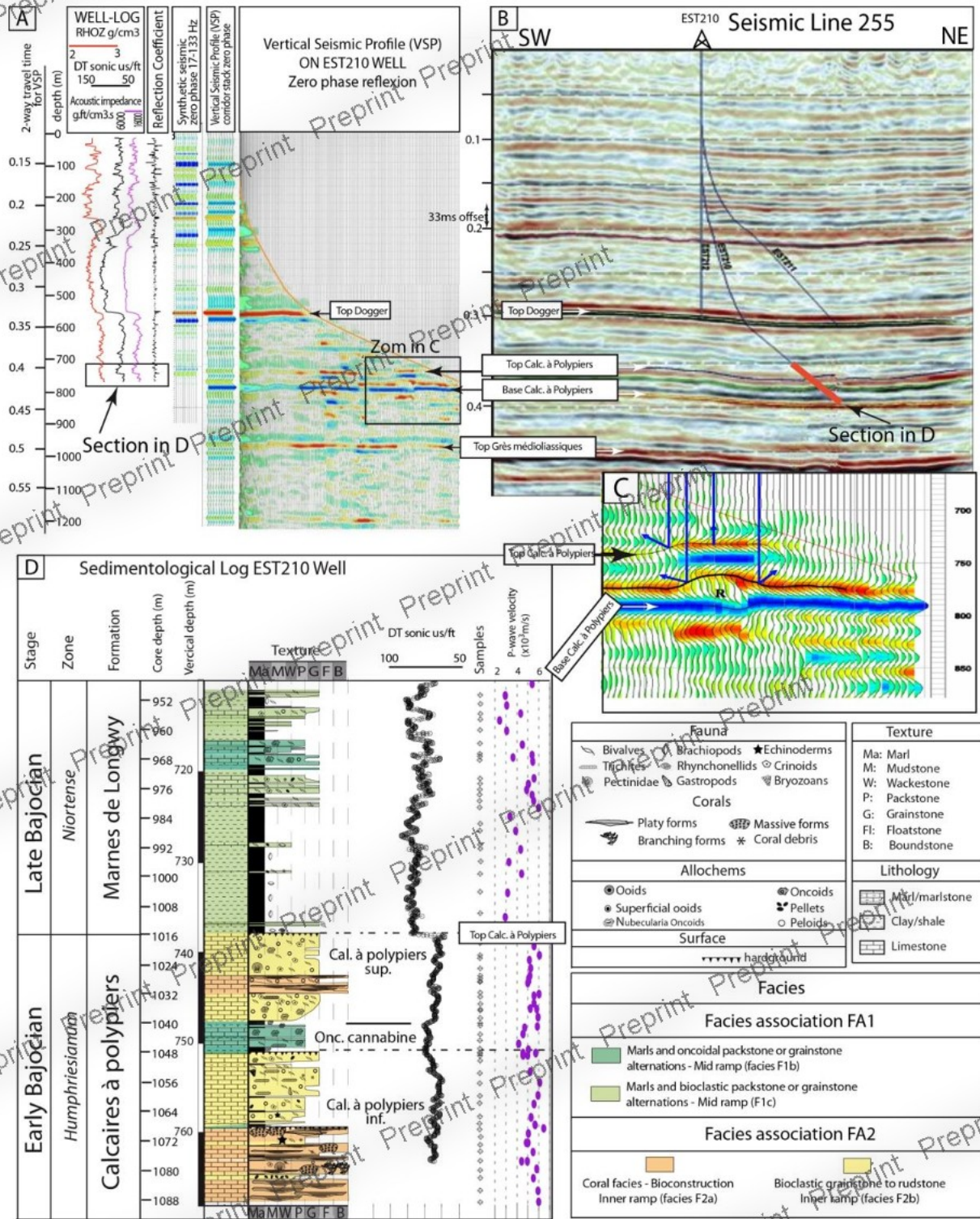


Fig. 14

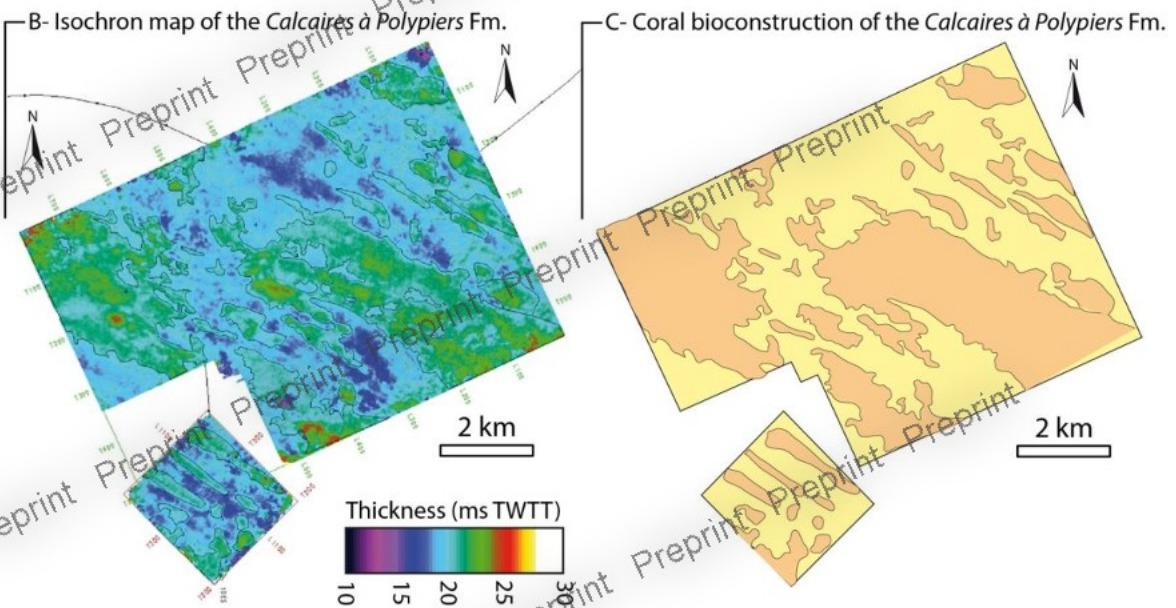
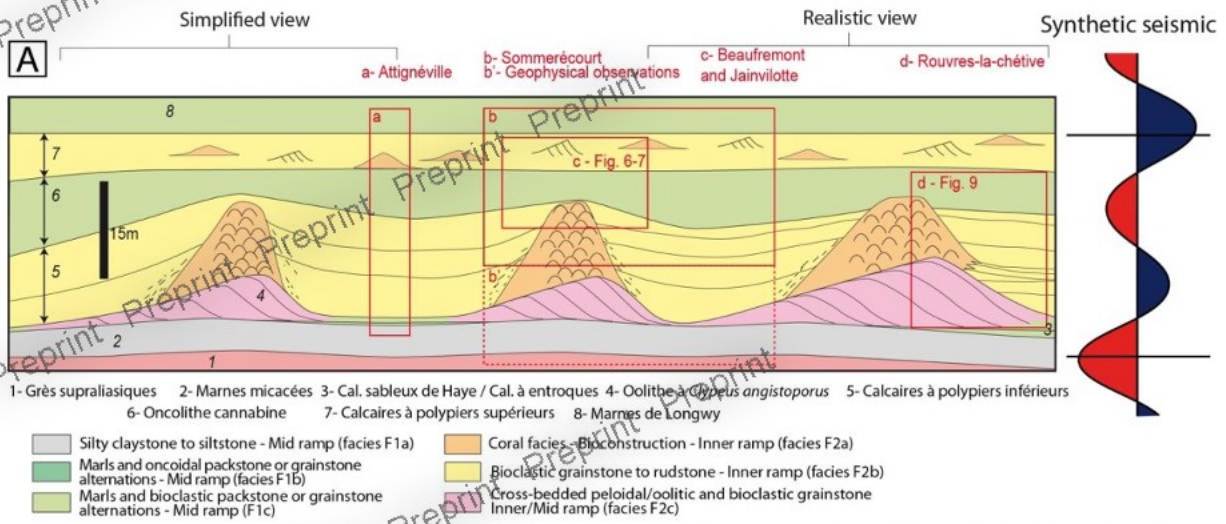


Fig. 15

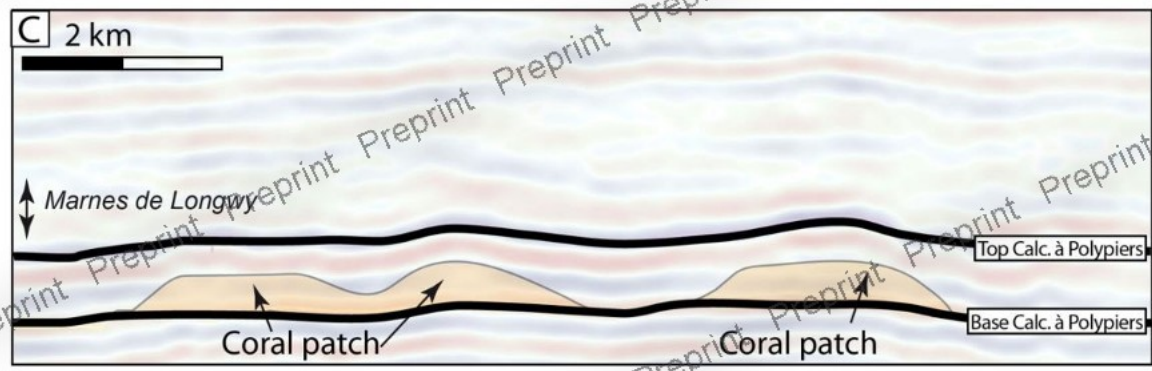
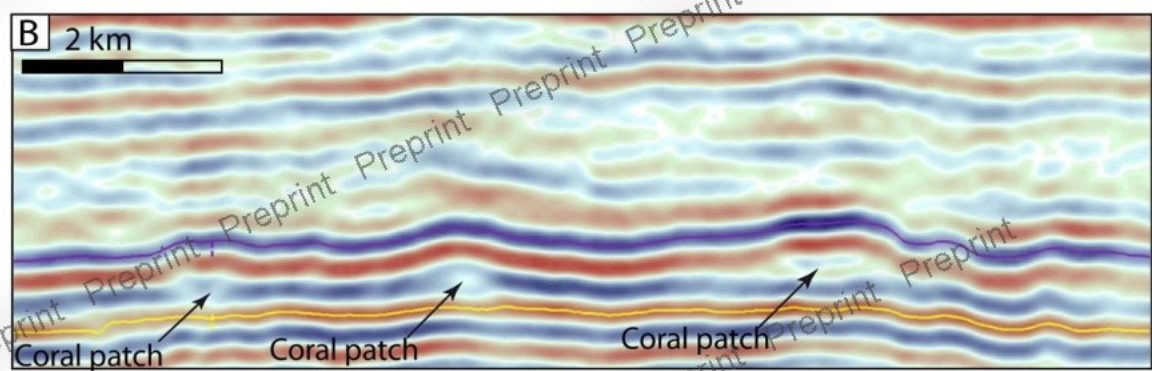
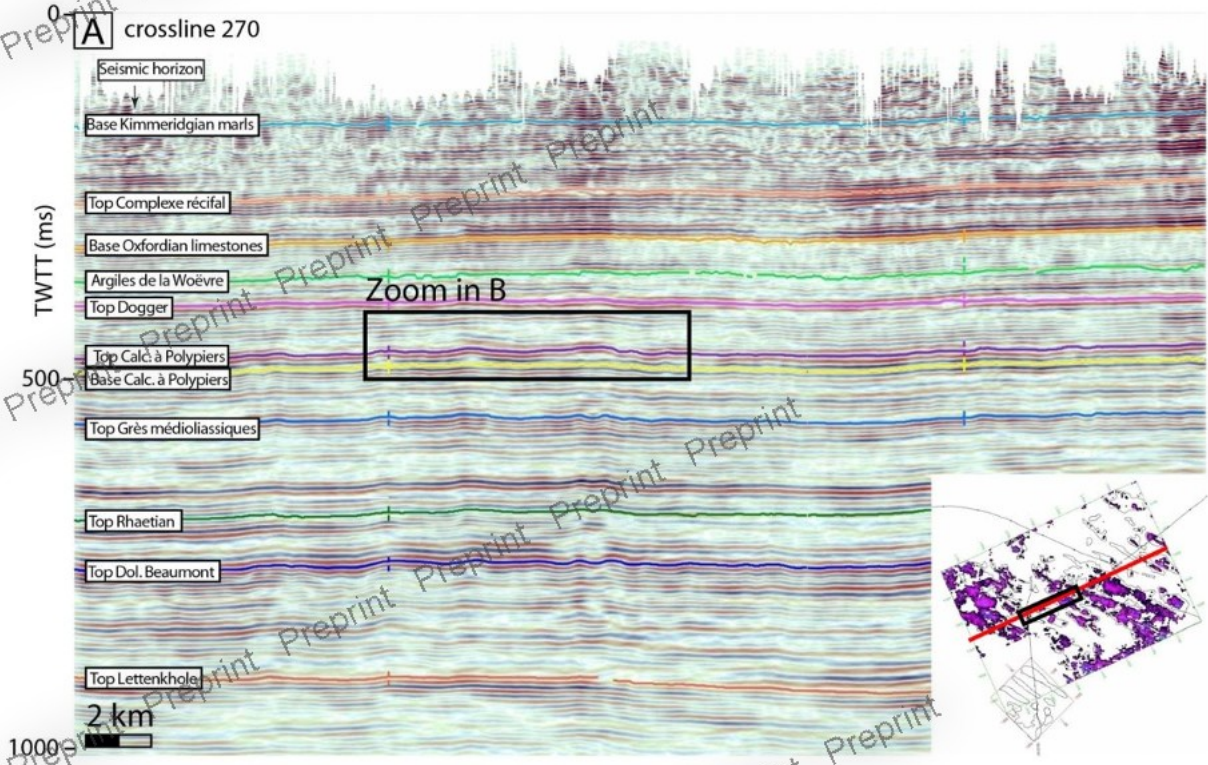
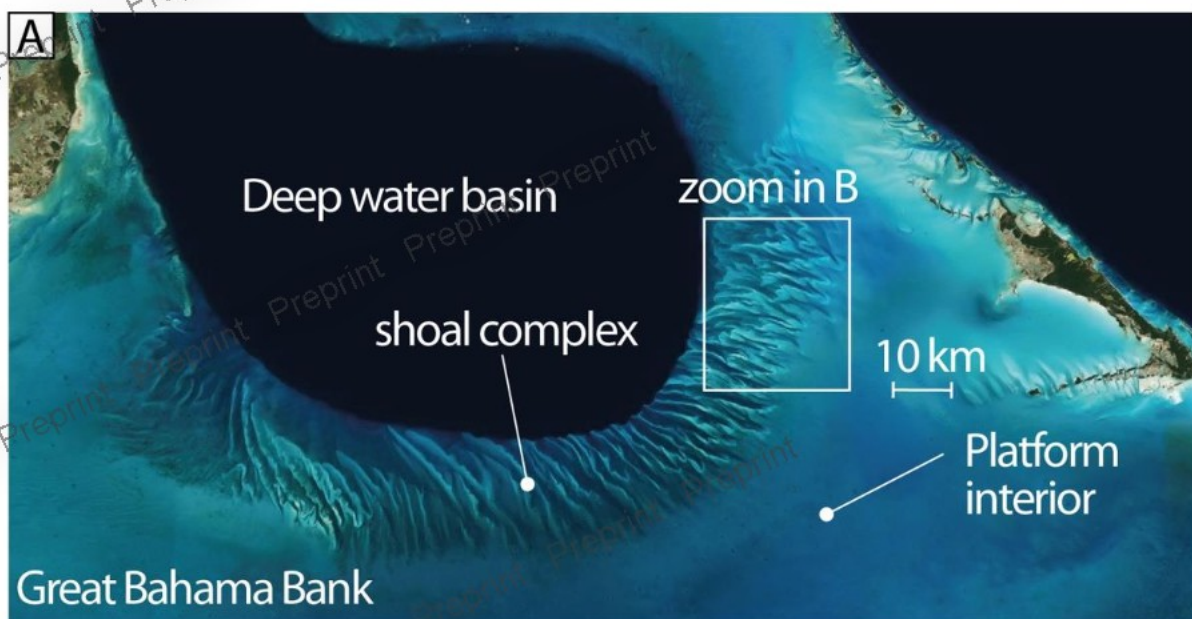
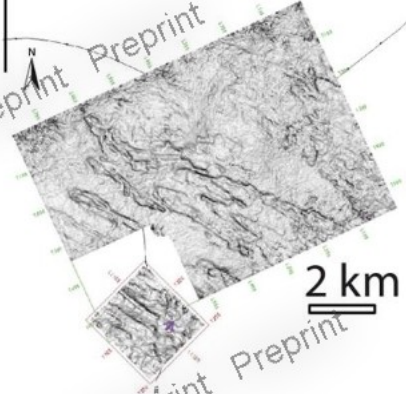


Fig. 16



C-Dip attribute map extracted on Top of Calc. à Polypiers Fm.



Bathymetry (m)

Fig. 17

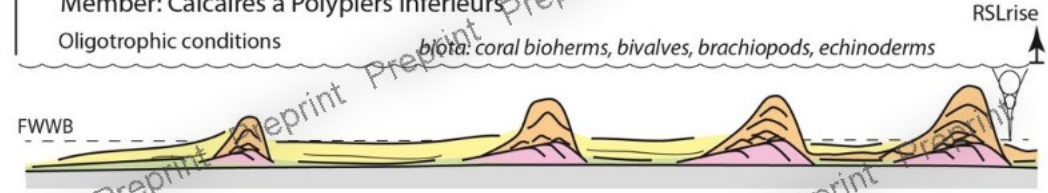
A- Silty claystone to siltstone - Outer ramp
 Climatic conditions: 15-20°C and humid
 Period: Early Bajocian - *discites* Zone
 Formation : Marnes micacées
 Mesotrophic conditions



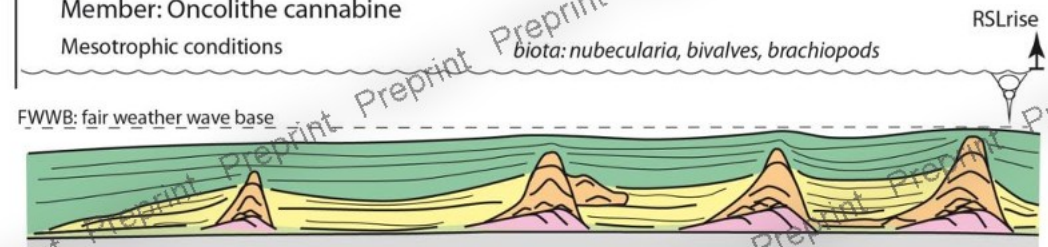
B- Early coral growth on the top of giant oo-bioclastic dunes - Mid to Inner ramp
 Climatic conditions: 20-30°C and humid
 Period: Early Bajocian - *laeviscula*, *propinquans*, *humphresianum* Zones
 Members: Oolites à *Clypeus angustiporus* and Calcaires à Polypiers inférieurs
 Oligotrophic conditions



C- Carbonate platform - Coral bioherms and bioclastic grainstone
 Climatic conditions: 20-30°C and humid
 Period: Early Bajocian - *humphresianum* Zone
 Member: Calcaires à Polypiers inférieurs
 Oligotrophic conditions
 biota: coral bioherms, bivalves, brachiopods, echinoderms



D- Carbonate platform - bioclastic and oncoidal facies
 Period: Early Bajocian - *humphresianum* Zones
 Member: Oncolithe cannabine
 Mesotrophic conditions
 biota: nubecularia, bivalves, brachiopods



- Coral facies - Bioconstruction (facies F2a)
- Bioclastic grainstone to rudstone (facies F2b)
- Cross-bedded peloidal/oolitic and bioclastic grainstone (facies F2c)
- Silty claystone to siltstone (facies F1a)
- Marls and oncoidal packstone or grainstone alternations (facies F1b)
- Marls and bioclastic packstone or grainstone alternations (F1c)

Fig. 18